

# Cerebellar Purkinje Cells Control Posture in Larval Zebrafish (*Danio rerio*)

Franziska Auer <sup>1</sup>, Katherine Nardone <sup>1</sup>, Koji Matsuda <sup>2</sup>, Masahiko Hibi <sup>2</sup>, David Schoppik <sup>1,3,\*</sup>

<sup>1</sup> Depts. of Otolaryngology, Neuroscience & Physiology, and the Neuroscience Institute, NYU Grossman School of Medicine

<sup>2</sup> Division of Biological Science, Graduate School of Science, Nagoya University, Japan

<sup>3</sup> Lead Contact

\* Correspondence: [schoppik@gmail.com](mailto:schoppik@gmail.com)

## ABSTRACT

**Cerebellar dysfunction leads to postural instability. Recent work in freely moving rodents has transformed investigations of cerebellar contributions to posture. However, the combined complexity of terrestrial locomotion and the rodent cerebellum motivate development of new approaches to perturb cerebellar function in simpler vertebrates. Here, we used a powerful chemogenetic tool (TRPV1/capsaicin) to define the role of Purkinje cells — the output neurons of the cerebellar cortex — as larval zebrafish swam freely in depth. We achieved both bidirectional control (activation and ablation) of Purkinje cells while performing quantitative high-throughput assessment of posture and locomotion. Activation disrupted postural control in the pitch (nose-up/nose-down) axis. Similarly, ablations disrupted pitch-axis posture and fin-body coordination responsible for climbs. Postural disruption was more widespread in older larvae, offering a window into emergent roles for the developing cerebellum in the control of posture. Finally, we found that activity in Purkinje cells could individually and collectively encode tilt direction, a key feature of postural control neurons. Our findings delineate an expected role for the cerebellum in postural control and vestibular sensation in larval zebrafish, establishing the validity of TRPV1/capsaicin-mediated perturbations in a simple, genetically-tractable vertebrate. Moreover, by comparing the contributions of Purkinje cell ablations to posture in time, we uncover signatures of emerging cerebellar control of posture across early development. This work takes a major step towards understanding an ancestral role of the cerebellum in regulating postural maturation.**

## INTRODUCTION

Cerebellar activity underlies proper posture and balance in vertebrates<sup>1-8</sup>. The cerebellum integrates sensory information from vestibular (balance), visual, and proprioceptive systems<sup>3</sup>. These sensations are transformed into precise adjustments in muscle tone and contraction allowing animals to resist destabilizing forces and maintain proper posture<sup>9</sup>. Disruptions to mature cerebellar function lead to instability, unsteady gait and a compromised sense of balance<sup>10</sup>.

Kinematic quantification by pose estimation in rodents<sup>11,12</sup> has opened a window into cerebellar contributions to postural behaviors in health and disease<sup>8,13,14</sup>. However, terrestrial gait and locomotion are complex. In contrast, the biophysical challenges of maintaining posture underwater are straightforward to define<sup>15,16</sup>. For example, larval zebrafish balance in the pitch axis (nose-up/nose-down) by timing locomotion to countermand gravity-induced destabilization<sup>17,18</sup> and by coordinated use of paired appendages (fins) and axial musculature (trunk)<sup>19</sup>. The small size and rapid development of the larval zebrafish allow high-throughput measurements of these movements from freely swimming subjects<sup>20</sup>.

The larval zebrafish is a powerful model to investigate cerebellar development and function<sup>21</sup>. Anatomically, the zebrafish cerebellum shares the same circuit structure as the mammalian cerebellum<sup>22</sup>. The zebrafish cerebellum is compartmentalized into regions with distinct response properties and output targets<sup>22-26</sup>. Multimodal representations were found in both cerebellar granule cells<sup>27,28</sup> and Purkinje cells, the output neurons of the cerebellar cortex<sup>25,29</sup>. Functional assays established a role for the larval zebrafish cerebellum in motor control, sensorimotor integration and predictive neural processing, particularly in response to visual input<sup>30-38</sup>. Finally, brain-wide imaging studies have established balance-relevant sensitivity in the cerebellum, identifying neurons that encode body angle and velocity<sup>39</sup> and neurons responsive to direct inner-ear stimulation<sup>40</sup>. Overwhelmingly, this work has been done in reduced or restrained preparations, limiting insight into the cerebellar contribution to natural behaviors.

Powerful new opto- and chemogenetic<sup>41</sup> approaches allow control of particular cerebellar cell types, reviewed in<sup>42</sup>. Recent work used such activation/inhibition to investigate cerebellar contributions to sensorimotor<sup>43-46</sup> and non-sensorimotor behaviors<sup>47-50</sup> in health and disease<sup>51-53</sup>. Both approaches come with technical hurdles: optogenetics requires targeting light to the cerebellum, while chemogenetics uses bioactive co-factors<sup>54</sup>. A chemogenetic approach to cerebellar control with a non-bioactive ligand would be a welcome advance, particularly to study posture without visual interference (i.e. in the dark). One path forward is to express the rat non-selective cation channel TRPV1 and its ligand capsaicin in zebrafish<sup>55</sup>. The endogenous zebrafish TRPV1 channel is capsaicin-insensitive<sup>56</sup>, so targeted expression of rat TRPV1 allows cell-type specific control: low-doses of capsaicin can activate sensory and hypothalamic neurons while high-doses are excitotoxic<sup>55</sup>. Capsaicin can be dissolved in water and is readily absorbed by freely-swimming larval zebrafish, sidestepping invasive procedures and the need for visible light. Finally, the conductance of a TRP channel is ~1000x that of a channelrhodopsin<sup>57</sup> suggesting that even low levels of TRPV1 expression will be biologically effective.

Here we used the TRPV1/capsaicin system to investigate the contribution of cerebellar Purkinje cells to postural behaviors as larval zebrafish swam freely in depth. Both activation and ablation of Purkinje cells could induce changes in

pitch axis posture. Ablation in older larvae resulted in bigger disruptions to posture, allowing inference of the functional consequences of cerebellar development. Furthermore, ablation of Purkinje cells in older larvae disrupted the coordination of trunk and paired appendages (fins), impairing vertical navigation. Finally, we could reliably decode pitch-tilt direction from patterns of Purkinje cell activity. Taken together our results establish a clear role for the cerebellum in larval zebrafish postural control, even during the earliest stages of development. More broadly, our work establishes a powerful new method to manipulate cerebellar output while performing quantitative high-throughput measures of unconstrained posture and locomotion. Our data are therefore a step towards defining an ancestral role for the highly-conserved cerebellum in postural control.

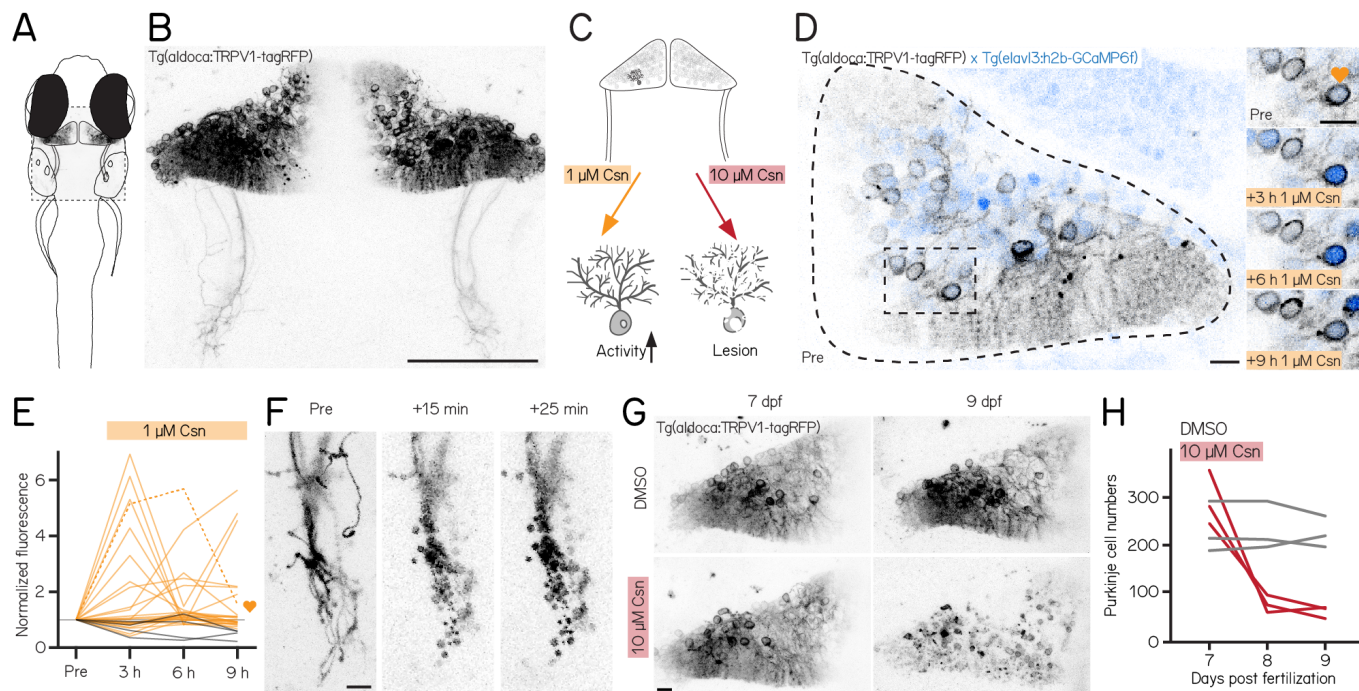


**Figure 1: A chemogenetic approach allows dose-dependent activation and lesion of Purkinje cells in the cerebellum.**

(A) Outline of a larval zebrafish with labelled Purkinje cells in the cerebellum. Gray rectangle corresponds to field of view in (B). (B) Confocal image of Purkinje cells in the cerebellum of a 7 days post-fertilization (dpf) *Tg(aldoca:TRPV1-tagRFP)* larvae. Scale bar 100  $\mu$ m. (C) Schematic of strategy for dose-dependent activation (yellow, left) or lesion (red, right) of Purkinje cells by addition of the TRP channel agonist capsaicin (Csn). (D) Confocal image of one cerebellar hemisphere of *Tg(aldoca:TRPV1-tagRFP)*; *Tg(elavl3:h2b-GCaMP6f)* larvae before, 3, 6, and 9 h after addition of capsaicin. Heart corresponds to the labelled trace in (E). (E) Normalized change in fluorescence following treatment with 1  $\mu$ M capsaicin in individual Purkinje cells as a function of time. Purkinje cells from *Tg(aldoca:TRPV1-tagRFP)*; *Tg(elavl3:h2b-GCaMP6f)* larvae (orange) and *Tg(elavl3:h2b-GCaMP6f)* control larvae (grey). (F) Timelapse images of Purkinje cell axons in *Tg(aldoca:TRPV1-tagRFP)* larvae immediately after addition of 10  $\mu$ M capsaicin. Scale bar 10  $\mu$ m. (G) Confocal images of cerebellar hemispheres of *Tg(aldoca:TRPV1-tagRFP)* larvae before (7 dpf, left) and after (9 dpf, right) treatment with 10  $\mu$ M capsaicin. Control larvae (DMSO, top) and lesion larvae (10  $\mu$ M capsaicin, bottom). Scale bar 10  $\mu$ m. (H) Quantification of Purkinje cell numbers of fish (n=3) from (G).

## RESULTS

### A new reagent for chemogenetic activation or ablation of Purkinje cells

We used a new reagent to control Purkinje cells: the transgenic line *Tg(aldoca:TRPV1-tagRFP)*. Fish in this line express rat TRPV1, a capsaicin-sensitive non-selective cation channel, exclusively in cerebellar Purkinje cells (Figures 1A and 1B). Endogenous zebrafish TRPV1 channels are insensitive to capsaicin<sup>56</sup>. Previous descriptions of rat TRPV1 in zebrafish sensory and hypothalamic neurons establish dose-dependent chemogenetic manipulation<sup>55</sup>. We expect low-doses of capsaicin to depolarize Purkinje cells (Figure 1C, left), while high-doses should be excitotoxic (Figure 1C, right).

First, we assayed capsaicin concentrations and incubation times to identify a dose that would achieve long-term depolarization without cell death. We co-expressed a nuclear-targeted calcium indicator, GCaMP6f (Figure 1D) in all neurons (*Tg(elavl3:h2B-GCaMP6f)*) for longitudinal imaging of neuronal activity. Previous work used 1  $\mu$ M of capsaicin for long-term activation<sup>55</sup>. We therefore imaged the cerebellum of *Tg(aldoca:TRPV1-tagRFP)*; *Tg(elavl3:h2B-GCaMP6f)* fish prior to and 3, 6, and 9 hours after 1  $\mu$ M capsaicin treatment (Figure 1D).

Prolonged exposure to a low dose of capsaicin increased cerebellar activity (Figure 1E). At each timepoint, TRPV1-expressing cells showed increased intensity relative to a pre-capsaicin baseline, while TRPV1-negative cells did not (Figure 1E) (3/6/9h post 1  $\mu$ M capsaicin: 32%/20%/20%/ TRPV1+ cells  $F/F_0 > 2$ ; 25/2 cells/animals vs 0%/0%/0%/ TRPV1-cells  $F/F_0 > 2$ ; 4/1 cells/animals).

Different cells showed increased activity at the 3, 6, and 9 hour timepoints, and the same cells were differentially active at different timepoints. We interpret this as evidence that 1  $\mu$ M of capsaicin could sporadically activate subsets of Purkinje cells. Notably, in one fish that had particularly strong tagRFP expression we observed a small number of neurons at the 9h timepoint with bright, speckled fluorescence suggestive of cell death (Figure S1B). We therefore set an upper limit of 6h of exposure to 1  $\mu$ M capsaicin for activation experiments.

Induced activation was reversible, even after prolonged exposure to 1  $\mu$ M of capsaicin. We tested whether the elevated patterns of neuronal activity that we observed in the presence of capsaicin would return to baseline by imaging cerebellar Purkinje cells in *Tg(elavl3:h2B-GCaMP6f)* before exposure, after 6h of 1  $\mu$ M capsaicin, and 40min after washout. Relative to baseline, fluorescent intensities increased after 6h, as in Figure 1E. Importantly, fluorescence returned to baseline levels after 40min of washout (Figure S1A) (6h post 1  $\mu$ M capsaicin: 40.9%/TRPV1+ cells  $F/F_0 > 2$ ; washout: 0%/TRPV1+ cells  $F/F_0 > 2$ ; 22/3 cells/animals). We conclude that capsaicin-induced activation is reversible after washout.

Exposure to high doses of capsaicin caused rapid axonal degeneration and cell death. We developed a protocol for Purkinje cell lesion: *Tg(aldoca:TRPV1-tagRFP)* larvae (without GCaMP6f) were imaged at 7 dpf, at 8 dpf after 1 h of 10  $\mu$ M capsaicin treatment and again at 9 dpf (Figure 1G). Timelapse imaging of the Purkinje cell axons showed rapid degeneration already 15min after capsaicin treatment started (Figure 1F). Cell numbers rapidly declined after 1h of 10  $\mu$ M capsaicin treatment and did not show any signs of recovery at 9 dpf (Figures 1G and 1H) (median (inter-quartile range); 7 dpf: control 213 (76) cells vs. pre lesion 282 (81) cells; 9 dpf: control 218 (49) cells vs. post lesion 68 (18) cells; 3/3 control animals/lesion animals).

Consistent with prior work in other cell populations<sup>55</sup>, we found that chemogenetic use of the capsaicin/TRPV1 system can be used to reversibly activate or rapidly ablate cerebellar Purkinje cells in larval zebrafish.

### Purkinje cells regulate postural control

We used our Scalable Apparatus to Measure Posture and Locomotion (SAMPL) to measure posture and locomotion in freely swimming zebrafish<sup>20</sup>. SAMPL is a high-throughput videographic approach that measures kinematic parameters of posture and locomotion from fish swimming in a predominantly vertical arena that encourages navigation in depth (Figures 2A and 2B). Larval zebrafish locomote in discrete bouts of rapid translation (Figure 2B, grey lines). To navigate up/down, fish sequence these bouts while maintaining a nose-up/nose-down pitch. Notably, climb/dive bouts are defined relative to the trajectory of the bout. Climb/dive bouts can therefore be initiated from either nose-up (positive) or nose-down (negative) postures.

Nose-up “climb” bouts (Figure 2E) engage both axial musculature of the body and the fins to produce a net upward trajectory while nose-down “dive” bouts (Figure 2J) rely on axial musculature alone and have a net downward trajectory<sup>19</sup>. Notably, posture after either climb or dive bouts tends to increase, a consequence of restorative rotations that counteract destabilizing torques<sup>18</sup>. SAMPL’s automated and high-throughput nature yields data with large numbers of observations. To ensure a focus on only the most meaningful differences, we adopted two stringent criteria for significance: p-values < 0.05, and an effect size of  $\geq 15\%$ . All p-values and effect sizes are reported in Tables 1 to 5.

We used the timing and capsaicin concentrations we had previously validated (Figure 1) to design two behavioral paradigms: one to activate and one to ablate cerebellar Purkinje cells. Experiments were done from 7–9 dpf, and began with a single day without perturbations; no differences between groups were observed during this time (Tables 1 and 2). Activation was then achieved by exposing *Tg(aldoca:TRPV1-tagRFP)*; *Tg(elavl3:h2B-GCaMP6f)* fish to two 6h periods of 1  $\mu$ M capsaicin while they swam freely in the dark (Figure 2C). Alternatively, Purkinje cells were ablated by exposing *Tg(aldoca:TRPV1-tagRFP)* fish to 10  $\mu$ M of capsaicin for 1h (Figure 2D). All fish were screened before experiments for comparable levels of tagRFP fluorescence and control and experimental groups were randomly selected. A single experimental repeat consisted of 1–3 apparatus run in parallel with fish from a single clutch of embryos (i.e. siblings). To maintain consistency with genotypes used for validation, the activation and ablation experiments had different backgrounds (i.e. the presence/absence of the *elavl3:h2B-GCaMP6f* allele). Because of background variation<sup>20</sup>, all comparisons were restricted to control vs. experimental groups within an experimental paradigm over the same time period. Across our datasets (Tables 1 to 3) we did not observe meaningful differences between the control and experimental groups in the pre-manipulation period. To avoid adding noise to our estimates of effect size, we therefore report comparisons between control and experimental groups after perturbation.

We did not observe global consequences for swimming: swim speed, swim frequency and bout duration were unaffected during Purkinje cell activation or after Purkinje cell lesion. Similarly, bout numbers (prior to filtering/excluding experiments) were not different between the control and activation (median (inter-quartile range) 1256 (883) bouts vs. 656 (1041) bouts; p-value 0.46) or lesion groups (1949 (1089) bouts vs. 1901 (795) bouts; p-value 0.84, Tables 1 and 2).

Climbing postures were perturbed after both activation and ablation of Purkinje cells. During activation, fish adopted more nose-up postures before and throughout climb bouts. We observed a shift towards more positive values across the distribution of postures before fish initiated a climb bout (Figure 2F). Across experimental repeats, the average climb posture of fish during depolarization was 29% higher than in control fish (Figure 2G, median [95% confidence interval]: 14.7° [14.0, 15.4]° vs. 19.0° [18.5, 19.7]°, p-value < 0.001, effect size: 29%). Similarly, after Purkinje cell lesion, the average climb posture increased 36% relative to controls (Figures 2H and 2I, 10.0° [9.5, 10.7]° vs. 13.6° [13.1, 14.3]°, p-value < 0.001, effect size: 36%).

We observed an unexpected decrease in the climb posture for control fish in the post-lesion period (from 18.0° [17.6, 18.4]° to 10.0° [9.5, 10.7], Table 2). We do not have an explanation for this particular change. Notably, if we assess the

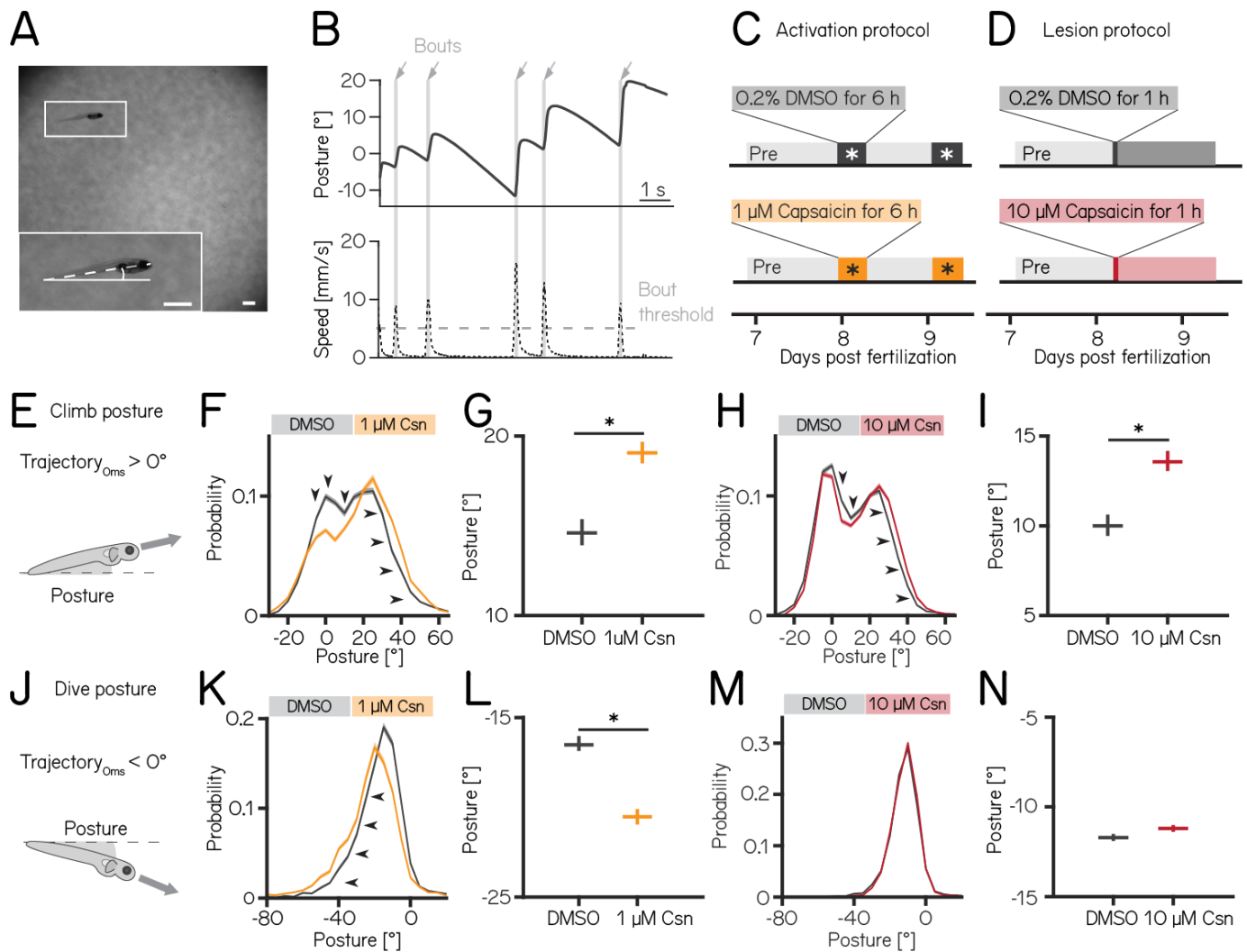


**Figure 2: Both chemogenetic activation and ablation of Purkinje cells disrupt postural stability.**

(A) Sample image of a freely-swimming zebrafish larva imaged from the side. Inset shows the larva at higher magnification view and its pitch, defined as the angle between the horizon (straight line) and the long axis of the body (dashed line). Scale bars 1mm. (B) Pitch angle (posture, top) and speed (bottom) as a function of time for one recorded epoch. Individual swim bouts (speed > 5 mm/s threshold) are highlighted in grey (arrows). (C) Timecourse for activation experiments between 7–9 dpf. Larvae received 1  $\mu\text{M}$  of capsaicin in 0.2% DMSO twice on days 8&9 for 6h each. (D) Timecourse for lesion experiments; larvae received a single dose of 10  $\mu\text{M}$  capsaicin in 0.2% DMSO for 1h on day 8. (E) Climbs are defined as a bout where the trajectory at peak speed took the fish nose-up ( $>0^\circ$ ). (F) Probability distribution of climb postures for control (black) and 1  $\mu\text{M}$  capsaicin treated larvae (yellow). Arrows denote the shift towards more nose-up postures. (G) Average climb posture of control and activated larvae (8 repeats/149 control fish; 8 repeats/155 1  $\mu\text{M}$  capsaicin treated fish; climb postures:  $14.7^\circ$  [14.0, 15.4] $^\circ$  vs.  $19.0^\circ$  [18.5, 19.7] $^\circ$ , p-value < 0.001, effect size: 29%, Wilcoxon rank sum test). (H) Probability distribution of climb postures for control (black) and 10  $\mu\text{M}$  capsaicin treated larvae (red). Arrows denote the shift towards more nose-up postures. (I) Average climb posture of control and lesioned larvae (14 repeats/110 control fish; 14 repeats/120 10  $\mu\text{M}$  capsaicin treated fish; climb postures:  $10.0^\circ$  [9.5, 10.7] $^\circ$  vs.  $13.6^\circ$  [13.1, 14.3] $^\circ$ , p-value < 0.001, effect size: 36%, Wilcoxon rank sum test). (J–N) Same as E–I, but for dive bouts (trajectory that took the fish in the nose-down direction). (L) Average dive posture of control and activated larvae (8 repeats/149 control fish; 8 repeats/155 1  $\mu\text{M}$  capsaicin treated fish; dive postures:  $-16.6^\circ$  [-16.9, -16.1] $^\circ$  vs.  $-20.5^\circ$  [-20.9, -20.1] $^\circ$ , p-value < 0.001, effect size = 24%, Wilcoxon rank sum test). (N) Average dive posture of control and lesioned larvae (14 repeats/110 control fish; 14 repeats/120 10  $\mu\text{M}$  capsaicin treated fish; dive postures:  $-11.7^\circ$  [-11.9, -11.5] $^\circ$  vs.  $-11.2^\circ$  [-11.4, -11.0] $^\circ$ , p-value = 0.002, effect size = -4%, Wilcoxon rank sum test). all data are shown as median with 95% confidence interval, \* indicates p-value < 0.05 and effect size  $\geq 15\%$

effect of adding 10  $\mu\text{M}$  capsaicin by comparing the magnitude of the relative difference between pre- and post-lesion periods, normalized to the pre-lesion period, we still see a significant difference (control vs lesion: -46% vs -26%). We conclude that, even when accounting for observed changes between control fish at 7 vs. 8 dpf, Purkinje cell ablation disrupts climb postures.

Dive bout postures were similarly perturbed after activation, but not ablation of Purkinje cells. Fish adopted more nose-down postures before and throughout dive bouts with a leftward shift of the distribution of postures before dive bouts (Figure 2K). Average dive bout posture was 24% more negative than in control animals (Figure 2L, median [95% confidence interval]:  $-16.6^\circ$  [-16.9, -16.1] $^\circ$  vs.  $-20.5^\circ$  [-20.9, -20.1] $^\circ$ , p-value < 0.001, effect size = 24%). Purkinje cell lesions at 7 dpf did not shift the average posture for dive bouts (Figures 2M and 2N  $-11.7^\circ$  [-11.9, -11.5] $^\circ$  vs.  $-11.2^\circ$  [-

11.4, -11.0]°, p-value = 0.002, effect size = -4%).

We interpret these data as evidence that Purkinje cell activity is crucial to ensure that posture during climbs and dives is maintained within a normal range.

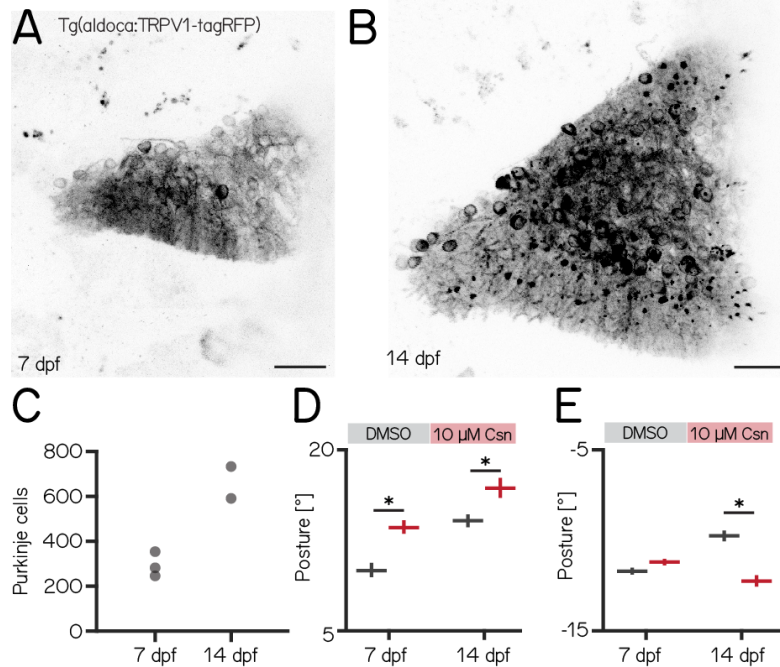


### Figure 3: Disruptions to postural stability after chemogenetic ablation of Purkinje cells are more pronounced in older fish.

**(A)** Confocal image of Purkinje cells in the cerebellum of a 7 dpf *Tg(aldoca:TRPV1-tagRFP)* larvae. Scale bar: 25  $\mu$ m. **(B)** Confocal image of Purkinje cells in the cerebellum of a 14 dpf *Tg(aldoca:TRPV1-tagRFP)* larvae. Scale bar: 25  $\mu$ m. **(C)** Increase in Purkinje cell numbers between 7 and 14 dpf. **(D)** Average climb bouts postures for 7 dpf control and lesion larvae (left) and 14 dpf control and lesion larvae (right). (14 dpf lesion: 7 repeats/48 control fish; 7 repeats/44 10  $\mu$ M capsaicin treated fish; climb postures: 14.3° [13.8, 14.8]° vs. 17.1° [16.2, 17.8]°; p-value < 0.001; effect size: 20%, Wilcoxon rank sum test). **(E)** Average dive bouts postures for 7 dpf control and lesion larvae (left) and 14 dpf control and lesion larvae (right). (14 dpf lesion: 7 repeats/48 control fish; 7 repeats/44 10  $\mu$ M capsaicin treated fish; dive postures: -9.8° [-10.1, -9.5]° vs. -12.3° [-12.6, -11.9]°; p-value < 0.001; effect size: 26%, Wilcoxon rank sum test). All data are shown as median with 95% confidence interval, \* indicates p-value < 0.05 and effect size  $\geq$  15%

### Loss of Purkinje cells in older fish results in more pronounced deficits to posture

Over the first two weeks of life, larval zebrafish morphology and postural control strategies develop considerably<sup>17</sup>. These changes are matched by similarly pronounced cerebellar growth<sup>58</sup> (Figures 3A and 3B). We observed that the number of Purkinje cells labelled in *Tg(aldoca:TRPV1-tagRFP)* roughly doubled between 7 and 14 dpf (Figure 3C, median (inter-quartile range) 7 dpf 282 (81); 14 dpf 662 (142)). The increase in cell numbers is also evidence that the *aldoca* promoter continued to drive expression at later stages, allowing us to perform comparative experiments.

Similar to lesions at 7 dpf, we did not observe any differences in swim speed, frequency or bout duration (Table 3). At 14 dpf, the effects of Purkinje cell lesions on posture were more widespread than at 7 dpf. We repeated our previous ablation experiments (Figure 2D) between 14–16 dpf, and analyzed climb (Figure 3D) and dive bouts (Figure 3E). Loss of Purkinje cells created more widespread behavioral deficits. Specifically, climb bout posture was increased by 20% after Purkinje cell lesion (median [95% confidence interval]: 14.3° [13.8, 14.8] vs. 17.1° [16.2, 17.8]; p-value < 0.001; effect size: 20%). At 14 dpf we also observed an effect on dive bout postures. After lesion dive bouts postures were 26% more negative (-9.8° [-10.1, -9.5]° vs. -12.3° [-12.6, -11.9]°; p-value < 0.001; effect size: 26%).

We conclude that, consistent with morphological growth, Purkinje cells of the cerebellum play a broader role in postural control at 14 dpf than at younger ages.

### Purkinje cells regulate speed-dependent fin engagement

To climb, larval zebrafish coordinate fin movements that generate lift with axial rotations that direct thrust (Figure 4A). The greater the axial rotation, the stronger the lift-producing fin movements; this relationship increases as larvae develop<sup>19</sup>. Our previous work suggested that Purkinje cells were necessary for such fin-body coordination<sup>19</sup>. Here, we observed that fin engagement is speed-dependent, with faster bouts producing greater lift for a given axial rotation (Figure 4B, left).

After Purkinje cell ablation, 14 dpf fish produced less lift than expected when they swam fast. We divided swim bouts into three different bins according to their peak speed (slow: 5–7.5mm/s; medium: 7.5–15mm/s; fast >15mm/s) for both control and fish treated with 10  $\mu$ M capsaicin. We parameterized the relationship between upward rotation and lift by fitting a line to swim bouts for each speed. After capsaicin exposure, the slopes of the medium and fast speed bins were significantly lower (Figure 4C), reflecting a loss of speed-dependent modulation (median [95% confidence interval]: slope slow: 0.028 [0.022, 0.034] mm/° vs. 0.028 [0.020, 0.037] mm/°, p-value = 0.51, effect size: 0%; slope medium: 0.053 [0.045, 0.061] mm/° vs. 0.029 [0.022, 0.032] mm/°, p-value < 0.001, effect size: -36%; slope fast: 0.066 [0.056, 0.080] mm/° vs. 0.046 [0.038, 0.056] mm/°, p-value < 0.001, effect size: -31%). Next, to determine if lift was fin-dependent, we amputated the fins and repeated our experiments. We observed a near total loss of lift at all speeds; regardless of the speed bin, the slope of the relationship between upward rotation and lift was indistinguishable from zero (slope slow: 0.032 [0.026, 0.039] mm/° vs. -0.005 [-0.008, -0.002] mm/°, p-value < 0.001; effect size: -50%; slope medium: 0.058 [0.050, 0.065] mm/° vs. -0.004 [-0.006, -0.003] mm/°, p-value < 0.001; effect size: -86%;

slope fast: 0.073 [0.059, 0.085] mm/° vs. 0.019 [0.015, 0.025] mm/°, p-value <0.001; effect size: -74%). Finally, we examined fin-body coordination in our 7 dpf activation and ablation datasets. In contrast to older larvae, we observed no meaningful changes after activation of Purkinje cells at 7 dpf. For Purkinje cell lesions at 7 dpf we found only the fin body coordination at fast bouts to be affected [Tables 1 and 2](#).

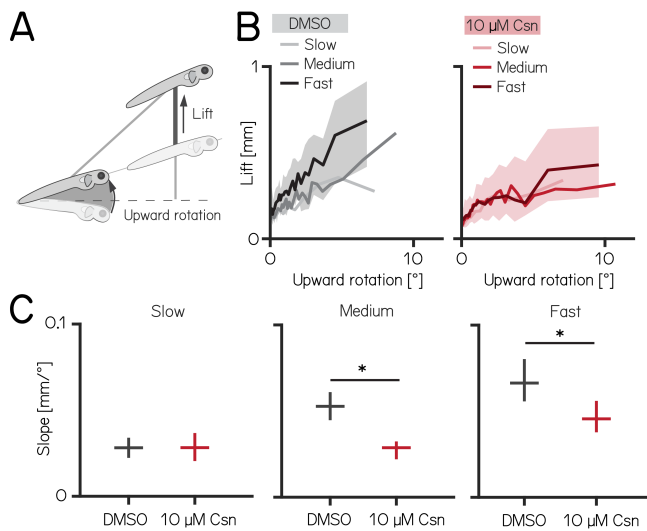


**Figure 4: Chemogenetic ablation of Purkinje cells disrupts fin-body coordination in a speed-dependent manner.**

**(A)** Larval zebrafish use two independent effectors (trunk and body) to climb. The contribution of each effector can be dissociated by the observed kinematics: changes to the angle of the trunk predict a trajectory for a particular bout (upward rotation). The actual position of the fish in depth at the end of the bout reveals the lift generated by the fins. A detailed kinematic examination of climbing, including fin ablations, is detailed in [19](#). **(B)** Coordination of fin and trunk engagement plotted as upward rotation against lift. Positive slopes reveal that larger rotations are coupled to greater fin engagement and greater changes in depth. The slope of this relationship becomes steeper for bouts with greater translational speed. Bouts from control (grey, left) and 10  $\mu$ M capsaicin treated larvae (red, right) are plotted at different swim speeds, shaded areas indicate inter-quartile range of the fast swim speeds. **(C)** Average slopes of lift/rotation curves for control and 10  $\mu$ M capsaicin treated larvae at different swim speeds. (8 repeats/15 control fish; 8 repeats/18 10  $\mu$ M capsaicin treated fish); slow: p = 0.51; medium: p < 0.001; fast: p < 0.001. Data are shown as median with 95% confidence interval. \* indicates p < 0.05 and effect size  $\geq$  15%

Our data show that loss of Purkinje cells disrupts the speed-dependent increase in fin-mediated lift in older, and to a lesser degree in younger fish. We interpret this finding as evidence that Purkinje cells are indispensable for normal coordination of the fins and body.

### Purkinje cells encode pitch direction at both individual and population levels

Our experiments establish that manipulations of Purkinje cells interfere with balance in the pitch axis. We therefore hypothesized that Purkinje cell activity would be modulated by nose-up/nose-down body tilts. We used Tilt In Place Microscopy (TIPM)<sup>20</sup> to measure the response of individual Purkinje cells ([Figure 5A](#)) to rapid pitch tilts. Briefly, fish are mounted on a mirror galvanometer and rapidly rotated to eccentric angles ([Figure 5B](#),  $\pm 30^\circ$  nose-up/nose-down).

We used *Tg(aldoca:GAL4);Tg(UAS:GCaMP6s)* to label Purkinje cells in the lateral parts of the cerebellum thought to receive vestibular input<sup>24,33,59</sup>. To facilitate identification of the same cells from volumes imaged at both  $\pm 30^\circ$ , we used doubly mono-allelic fish and screened for sparse expression of Purkinje cells. In total, we imaged 43 Purkinje cells from 8 fish. Of those, 31 cells could be reliably identified at  $\pm 30^\circ$  and were included in the analysis.

Individual Purkinje cells showed either directionally-tuned ([Figure 5C](#), n=18) or untuned ([Figure 5D](#), n=13) patterns of responses. Tuned cells were distributed throughout the lateral cerebellum ([Figure 5E](#)), and showed a slight preference for nose-down stimuli (12 vs. 6, [Figure 5F](#)). We did not observe any systematic differences in the response properties across each experiment from untuned cells ([Figure 5G](#)).

While untuned cells did not show overt directional preferences, pooling their responses allowed decoding of stimulus direction. We were motivated to model decoding because principal component analysis of the integral of the full responses on each trial from untuned neurons showed near-complete segregation of trial types ([Figure 5H](#)). To assay whether there was indeed directional information we trained a decoder (support vector machine) and tested its accuracy on pseudo-populations of different sizes ranging from 3 - 13 cells ([Figure 5I](#)). Training and test trials were different to avoid over-fitting. Pseudo-populations with more than 3 cells achieved accurate decoding well above chance levels (determined by shuffling trial identity) (median (inter-quartile range) accuracy: 3/5/7/10/13 cells: 0.78 (0.68-0.91) / 0.88 (0.70-0.88) / 1 (0.84-1) / 1 (0.97-1) / 1 (1-1)).

Older larvae showed additional changes to dive postures after Purkinje cell lesions. We therefore tested if: (1) Purkinje cells in older larvae exhibited differences in the numbers or direction of tuned cells or (2) if population-level decoding accuracy changed. We performed longitudinal TIPM, sampling from zebrafish larvae at 7 and 14 dpf. To improve throughput, we recorded the responses upon return from  $\pm 19^\circ$  stimuli ([Figure S2A](#)) (7 dpf: 138/11 cells/fish; 14 dpf: 90/7 cells/fish; of those 23/3 cells/fish were imaged at both timepoints); previous work established that responses upon return to baseline are highly correlated with the response at the eccentric position<sup>60</sup>. We observed increased fluorescence relative to baseline values in 7 dpf and 14 dpf Purkinje cells upon return from  $\pm 19^\circ$  steps ([Figure S2B](#) and [Figure S2C](#)). To analyze directional tuning we compared the maximum fluorescence in the first second after return to baseline. The relative number of tuned cells per fish was comparable between 7 and 14 dpf larvae ([Figure S2D](#); median (interquartile range) at 7 dpf: 7 (6-34)%; 14 dpf: 8 (2-19)%; p-value = 0.7763). While most cells were not directionally selective, the preferred direction of tuned cells was different at 7 and 14 dpf: at 7 dpf more Purkinje cells were nose-down tuned (2/31 up/down) but at 14 dpf more cells were nose-up tuned (11/3 up/down [Figure S2E](#); Fisher's exact test, p-value < 0.001).

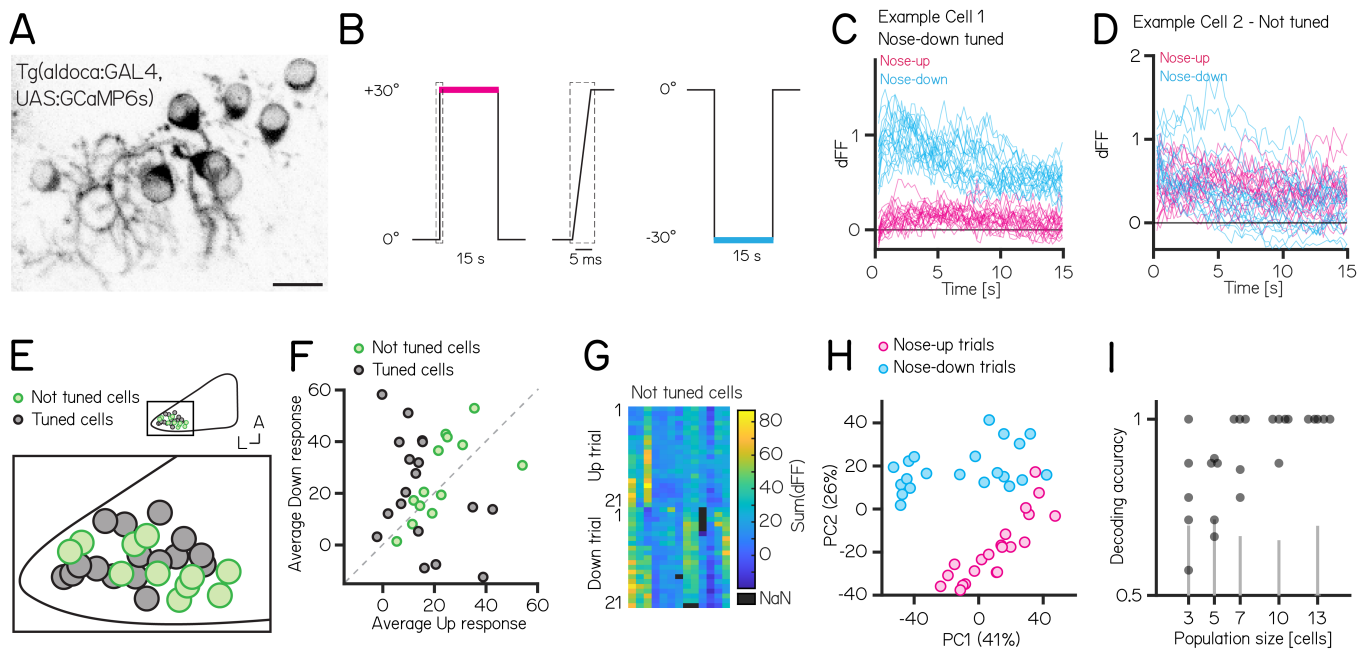


**Figure 5: Activity in larval zebrafish Purkinje cells can differentiate nose-up from nose-down pitch both individually and collectively.**

(A) 2-photon image of Purkinje cell somata expressing a calcium indicator in the *Tg(aldoca:GAL4);Tg(UAS:GCaMP6s)* line. Scale bar 10  $\mu\text{m}$ . (B) Pitch tilt stimuli consisted of rapid galvanometer steps for 15 seconds in the nose up (+30°, pink) and nose-down (-30°, blue) direction. Inset in dotted rectangle shows the near-instantaneous timecourse of the step. (C) Example responses (n=42) from a single Purkinje cell sensitive to nose-down pitch (blue) but not nose-up (pink). (D) Example responses (n=42) from a single Purkinje cell without directional selectivity. (E) Superimposed positions of Purkinje cell somata within a single cerebellar hemisphere; no obvious topography separates tuned (black, n=16) and untuned (green, n=11 |directionality index| < 0.35) cells. (F) Averaged integrated response (dFF) for individual cells over the 15 second stimulus plotted for nose-up vs. nose-down stimuli, colored by tuned (black) and untuned (green). (G) Heatmap of integrated response (dFF) for 13 untuned neurons on 21 up/down tilts. (H) Principal component analysis of integrated responses for untuned neurons for each of 21 up (pink) and 21 down (blue) trials. (Percentage of variance explained) (I) Performance of a support vector machine for binary classification of up/down tilt using integrated responses from increasing numbers of untuned neurons. Dots are different sets of neurons, gray lines shows the spread of performance from shuffled up/down identity (median (interquartile range) accuracy: 3/5/7/10/13 cells: 0.78 (0.68-0.91) / 0.88 (0.70-0.88) / 1 (0.84-1) / 1 (0.97-1) / 1 (1-1)).

We next assayed accuracy of directional encoding of untuned cells. We performed principal component analysis of untuned cells at 7 (Figure S2F) and 14 dpf (Figure S2G) and tested decoding accuracy on the untuned cells of individual fish at 7 and 14 dpf. We did not observe differences in decoding accuracy between 7 and 14 dpf larvae (Figure S2H; median (interquartile range) 7 dpf: 0.68 (0.63-0.83); 14 dpf: 0.73 (0.65-0.79); p-value = 0.9468).

We conclude that cerebellar Purkinje cells can encode pitch direction both at the single neuron and population levels with similar encoding accuracy in young and older larvae.

## DISCUSSION

We used a novel chemogenetic tool to define the role of cerebellar Purkinje cells in postural behavior as larval zebrafish swam freely in depth. Activation of Purkinje cells could induce changes in pitch axis (nose-up/nose-down) posture. Purkinje cell ablation disrupted posture, with broader effects in older larvae. Ablation disrupted fin-body coordination responsible for proper climbing. Finally, we could reliably decode pitch-tilt direction from patterns of Purkinje cell activity. We did not observe developmental changes in population coding of direction but found a shift in the tuning direction of Purkinje cells. Taken together our results establish a role for the cerebellum in postural control even during the earliest stages of larval zebrafish development. Our work establishes a powerful new method that combines bidirectional manipulation of cerebellar output and quantitative high-throughput measures of unconstrained posture and locomotion.

### Contributions of Purkinje cells to posture

While activation and ablation manipulations both produced biologically meaningful behavior changes, the two experiments were run with different genetic backgrounds and on different generations of the SAMPL apparatus. Consequently, our ability to define precisely what role Purkinje cells play in balance behaviors in larval zebrafish is limited. Activation experiments are particularly laborious as they require thorough pre-screening to ensure adequate brightness levels to achieve sufficient depolarization without excitotoxicity. Given that the primary purpose of this series of experiments was to establish TRPV1-mediated manipulation of Purkinje cells as a means to investigate postural control, it is beyond the scope of the work to repeat the experiments. Nonetheless, we consider the findings individually

below in the context of prior work.

Purkinje cell ablations disrupt postural stability. Importantly, the differences we observed were more widespread in older larvae, underscoring the developmental importance of Purkinje cells for balance. Purkinje cell output is inhibitory<sup>61,62</sup>, Purkinje cells in the lateral cerebellum project to vestibular nuclei<sup>24,33</sup>, and Purkinje cells are tonically active<sup>63,64</sup>. We propose that the net effect of Purkinje cell loss would be disinhibition of target nuclei responsible for encoding posture and parameterizing corrective pitch-axis behaviors. While the precise nature of the transformation between larval zebrafish pitch and posture control kinematics is not yet known, loss of cerebellar-targeted nuclei can disrupt postural behaviors<sup>19,65</sup>.

The effects of ablations became more widespread in older larvae. During early development, larval zebrafish grow in volume by roughly an order of magnitude and shift their postural control strategies to better climb/dive as they navigate in depth<sup>17,19</sup>. Unlike climb bouts, disruptions to postural stability during dives only emerge at 14 dpf. As activation of Purkinje cells produced meaningful disruptions during dives at 7 dpf, we infer that the delayed emergence of ablation effects does not reflect incomplete integration of Purkinje cells into dive-control circuits. Instead, we propose that the delay reveals the functional emergence of Purkinje cell control of dives across development. Notably, the basal posture during dive bouts decreases in older control animals (Figure 3E) — ablation shifts the posture comparable to its younger state. Future work with our system enables testing of the hypothesis that Purkinje cell output plays a role in setting the postures older fish adopt during dives.

Purkinje cell activation also disrupts postural stability. Intriguingly, activation broadened the distribution of observed postures in the same way as ablation. Our imaging assay established that 1  $\mu$ M of capsaicin would stochastically activate subsets of Purkinje cells. This stochasticity could reflect normal fluctuations in basal levels of activity, or it could arise from cells going in and out of depolarization block<sup>66</sup>. Synchronized/precisely-timed Purkinje cell output is thought to shape movements<sup>67-72</sup>, though perhaps not for all behaviors<sup>73</sup>. Our imaging suggests that the set of Purkinje cells activated at any one moment in time is limited and random. We therefore propose that the net effect of 1  $\mu$ M of capsaicin is ultimately disruptive to Purkinje cell synchrony, and thus likely disruptive. Future work could test this hypothesis by intracellular recording from cerebello-recipient populations like the vestibular nuclei<sup>74,75</sup>.

Previously, we reported that larval zebrafish coordinate their fins and trunk to climb effectively<sup>19</sup>. The relationship between trunk-mediated changes to trajectory (upward rotation) and fin-mediated lift depends on locomotor speed. Here we observed that after Purkinje cell loss, speed-dependent increases in lift with greater trunk rotation are disrupted (Figure 4C). As we did not observe any change to locomotor speed after ablation (Tables 1 to 3), we infer that Purkinje cell loss disrupts speed-dependent coordination for climbing. These results extend our original report where a lower-throughput method (photoablation) suggested that Purkinje cell loss impacted the fin-trunk relationship<sup>19</sup>. In larval zebrafish, the neuronal substrates for axial speed control<sup>76-81</sup> and fin engagement<sup>82</sup> are known. The potential for whole-brain imaging in larval zebrafish<sup>35</sup>, particularly with high-speed voltage indicators<sup>83</sup> and cutting-edge modeling approaches<sup>84</sup>, stands to reveal how Purkinje cell activity comes to coordinate body and fin movements. Importantly, since our behavioral data suggest that Purkinje cell activity impacts fin-trunk coordination more strongly in older larvae, longitudinal approaches will be key to understanding the developmental changes to cerebellar signaling that underlie effective coordination of trunk and limbs.

### Encoding strategies for body tilt stimuli

Purkinje cell activity reflects both sensory and motor inputs. One limitation of TIPM is that larvae are immobilized in agarose during tilts. Consequentially, our measurements of Purkinje cell activity are artificially constrained. Nonetheless, a subset of Purkinje cells were unambiguously direction-selective, and a simple decoder could use the activity of non-selective cells to differentiate tilt direction. We infer that vestibular information directly related to pitch axis posture is represented by the Purkinje cell population targeted in our ablation/activation experiments, consistent with broader imaging of cerebellar responses to body tilt<sup>39,40</sup>. Similar to the behavior results, we observed an asymmetry in the tuning direction of Purkinje cells at 7 dpf, with more cells being tuned to the nose-down direction. This asymmetry shifted between 7 and 14 dpf, suggesting developmental changes in how navigation in the pitch axis is processed in the cerebellum. These changes underscore the importance of longitudinal measurements of Purkinje cell activity across early development to understand emergent control of posture.

The ability to decode tilt direction from the collective activity of “untuned” Purkinje cells suggests a role for population coding. Such mechanisms have been proposed for head/body motion<sup>85</sup> and eye movements<sup>73,86</sup> in the primate cerebellum. Population coding requires that multiple Purkinje cells converge onto downstream targets, which is well-established in cerebellar target nuclei<sup>68,87</sup>. In larval zebrafish, Purkinje cells involved in locomotion converge on eurydendroid cells; electrophysiological recordings confirm a many-to-one convergence scheme that could similarly support population coding<sup>25</sup>. Vestibular-sensitive cells are located in the lateral cerebellum<sup>39,40</sup>, which projects to hindbrain regions that contain vestibular nuclei<sup>58</sup>. Comparing activity of vestibular nucleus neurons involved in tilt-driven behaviors<sup>74,88,89</sup> before/after TRPV1-mediated ablation would speak to the collective contributions of Purkinje cells.

### TRPV1/capsaicin as a tool to study cerebellar contributions to behavior

Our use of TRPV1/capsaicin complements a modern suite of molecular tools to target cerebellar Purkinje cells<sup>42</sup>. In fish, different experiments have used opsins to excite / inhibit cerebellar Purkinje cells with exceptional temporal precision, establishing functional topography<sup>24</sup> and an instructive role in learning<sup>25</sup>. TRPV1/capsaicin is a well-validated



approach<sup>55</sup> that permits parametric (i.e. dose-dependent) activation/ablation with a single transgenic line. It does not require light, facilitating dissociation of vestibular from visual contributions without requiring genetically-blind fish as in other studies using excitatory opsins<sup>90</sup>. Finally, chemogenetic approaches such as TRPV1/capsaicin permit prolonged experimentation in freely-moving animals, allowing us to collect large kinematic datasets necessary to rigorously study posture and locomotion.

Considerable progress has been made in recent years using new tools<sup>8,11-14</sup> and new perspectives<sup>91</sup> to understand the cerebellar contributions to sensorimotor<sup>43-46</sup> and non-sensorimotor behaviors<sup>47-50</sup> in health and disease<sup>51-53</sup>. Underlying this considerable progress is an ever-improving ability to manipulate the cerebellum without compromising rigorous measures of behavior. Here — in support of similar goals — we validated a new chemogenetic approach (TRPV1/capsaicin-mediated activation and ablation) compatible with a high-throughput paradigm to measure behavior in freely swimming larval zebrafish (SAMPL). Our data uncover expected signatures of cerebellar contributions to posture and coordination, establishing the validity of our approach. Further, by comparing the impact of Purkinje cell ablation in time, we leverage the rapid maturation of the zebrafish to open a window into cerebellar control of posture and coordination across development. Our approach establishes a path forward for the larval zebrafish model to contribute to cerebellar mechanisms of postural control. The cerebellum emerged early in the evolution of vertebrates, when vertebrate life was underwater. Our work establishes a powerful tool to investigate ancient organizing principles of cerebellar function.

## MATERIALS AND METHODS

### Fish Care

All procedures involving zebrafish larvae (*Danio rerio*) were approved by the Institutional Animal Care and Use Committee of New York University. Fertilized eggs were collected and maintained at 28.5°C on a standard 14/10 hour light/dark cycle. Before 5 dpf, larvae were maintained at densities of 20-50 larvae per petri dish of 10 cm diameter, filled with 25-40 mL E3 with 0.5 ppm methylene blue. After 5 dpf, larvae were maintained at densities under 20 larvae per petri dish and fed cultured rotifers (Reed Mariculture) daily.

### Fish Lines

To generate the *Tg(aldoca:TRPV1-TagRFP)* line, the 5-kbp aldolase Ca (*aldoca*) promoter<sup>92</sup> and a gene cassette that includes TRPV1-Tag1RFP cDNA, rabbit beta-globin intron, and the SV40 polyadenylation signal (pAS) in pT2-4xUAS:TRPV1-RFP<sup>55</sup> were subcloned into the Tol2 vector pT2KDest-RfaF<sup>93</sup> by the Gateway system (pT2K-aldoca-TRPV1-Tag1RFP-pAS). To establish stable transgenic lines, Tol2 plasmid and transposase mRNA (25 ng/ µl each) were injected into one-cell-stage embryos.

The resulting *Tg(aldoca:TRPV1-tagRFP)* stable line allowed us to express the mammalian capsaicin-sensitive cation channel TRPV1 and the red fluorophore tagRFP in cerebellar Purkinje cells. Before exposure to capsaicin, fish were screened to ensure similar levels of tagRFP expression. We measured neuronal activity using a genetically-encoded calcium indicator, *Tg(UAS:GCaMP6s)*<sup>78</sup>, driven by *Tg(aldoca:GAL4)*<sup>94</sup>, or the *Tg(elavl3:h2B-GCaMP6f)* line<sup>95</sup>.

### Confocal imaging of TRPV1-mediated activation / lesion

Images were collected using a Zeiss LSM800 confocal microscope using a 20x 1.0NA water immersion objective. Larvae were mounted in 2% low melting point agar (catalog #16520, Thermo Fisher Scientific) in a dorsal up position. Anatomical images were acquired from fish anesthetized with 0.2 mg/ml ethyl- 3-aminobenzoic acid ethyl ester (MESAB, catalog # E10521, Sigma- Aldrich). To activate TRPV1-expressing Purkinje cells, fish were treated with 1 µM capsaicin in 0.2% DMSO in E3. To lesion Purkinje cells, fish were exposed to 10 µM capsaicin in 0.2% DMSO in E3. Control fish were treated with 0.2% DMSO in E3. Agar was removed around the tip of the tail to facilitate drug delivery. Fish were mounted throughout functional imaging experiments and kept in temperature controlled incubators between timepoints. Confocal images were analyzed in Fiji<sup>96</sup>; ROIs were drawn on nuclei of randomly selected Purkinje cells, which were then re-identified at each time point. Fluorescence for each cell and time point was normalized to the pre-capsaicin value.

To image the anatomy of Purkinje cells exposed to 10 µM of capsaicin across time, the cerebellum was imaged at 7 dpf from fish mounted as above. Fish were unmounted and kept in E3 medium until the next day (8 dpf). At 8 dpf, fish were placed in 0.2% DMSO in E3 (control) or 10 µM capsaicin in 0.2% DMSO in E3 for 40-60min, and imaged again after 1h of recovery in E3 post-treatment. Fish from both groups were imaged again at 9 dpf. Confocal images were analyzed in Fiji and Purkinje cell somata were counted in both hemispheres of the cerebellum.

### Zebrafish behavior recordings

All behavior was measured using the Scalable Apparatus for Measuring Posture and Locomotion (SAMPL) apparatus, consisting of a chamber where larvae could swim freely, an infrared illuminator, a camera, and software to process video in real time. A comprehensive description of the apparatus is contained in<sup>20</sup>. Here we briefly describe the specific details of our experiments. Larvae were transferred to chambers at densities of 3-8 fish per chamber for 7 dpf experiments or 1-4 fish per chamber for 14 dpf experiments containing 25-30 ml of E3 or 0.2% DMSO / 1 µM capsaicin for activation experiments. After 24 h, behavior recordings were paused for 30-60 minutes for feeding (feeding pause) and 1-2 ml of rotifer culture was added to each chamber. Larvae were removed from the apparatus after 48h.

To monitor behavior before/during Purkinje cell activation, 7 dpf larvae were placed in chambers with E3. At 8 & 9 dpf, control fish were placed in 0.2% DMSO in E3 and the condition fish were placed in 1 µM capsaicin in 0.2% DMSO

in E3 for 6h. Video was sampled at 40Hz in constant darkness. Control: 9709 bouts (63% climb bouts)/149 fish/8 experimental repeats; Activation: 9734 bouts (61% climb bouts)/155 fish/8 experimental repeats;

To monitor behavior before/after Purkinje cell lesions, 7 dpf/14 dpf larvae were placed in the chambers with E3. After feeding at 8 dpf/15 dpf, fish were placed in petri dishes with 0.2% DMSO in E3 (control) or 10  $\mu$ M capsaicin in 0.2% DMSO in E3 for 40-60min. Fish were then returned to the chambers in E3 and behavior recording was started. Video was sampled at 160Hz in constant darkness. 7 dpf lesions: Control: 17941 bouts (61% climb bouts)/110 fish/14 experimental repeats; Lesion: 17863 bouts (58% climb bouts)/120 fish/14 experimental repeats; 14 dpf lesion: Control: 10853 bouts (59% climb bouts)/48 fish/7 experimental repeats; Lesion: 10832 bouts (55% climb bouts)/44 fish/7 experimental repeats;

Pectoral fin amputations were performed at 13 dpf. Two length-matched siblings were anesthetized in 0.2 mg/ml ethyl- 3-aminobenzoic acid ethyl ester (MESAB, catalog # E10521, Sigma- Aldrich) simultaneously and mounted in 2% low-melting temperature agar. Visualized under a stereomicroscope (Leica M80, 20x/12 eyepieces, 1.0x objective), the two pectoral fins from one larva were removed by pulling the base of the fin at the scapulocoracoid laterally with #5 Dumont forceps. After amputation, both fish were freed from the agar and allowed to recover in E3 until the next day, at which point half of the amputated and control fish were randomly selected for Purkinje cell lesions. Lesions were performed as above and behavior recorded for 48h. Behavior was recorded at a sampling rate of 160Hz with a 14/10h light-dark cycle. Control: 1572/5120/5354 (slow/medium/fast) bouts/15 fish/8 experimental repeats; Purkinje cell lesion: 1785/6229/4299 (slow/medium/fast) bouts/18 fish/8 experimental repeats; Fin amputation: 1938/6295/4911 (slow/medium/fast) bouts/17 fish/8 experimental repeats.

### Behavior analysis

Comprehensive descriptions of behavioral kinematics and baseline data for different genetic backgrounds are detailed in<sup>20</sup>. Here we describe the specific parameters used for our experiments. Behavior data were analyzed using custom-written software in MATLAB (Mathworks, Natick MA), which extracted individual swim bouts from the raw data (x/z position and pitch angle as a function of time). Only bouts during the circadian day were analyzed. Experimental repeats consisted of data collected across multiple SAMPL boxes from a single clutch of fish; the number of fish available determined how many apparatus were used (1-3). For comparisons across conditions (e.g. activation/control), fish from one clutch were randomly split into control and condition groups. As bout number is the fundamental unit of kinematic analysis, and different numbers of fish available would yield different numbers of bouts, we bounded our experiments to allow comparison across repeats. Specifically, if an experimental repeat contained less than 650 bouts it was excluded. Between 22-27% of lesion experimental repeats contained less than 650 bouts and were not included in the analysis. For the activation experiments 56% (10 of 18) of experimental repeats were excluded with the 650 bouts threshold due to shorter recording times a higher fraction of experiments contained less than the threshold number of bouts. In subsequent analyses, the number of analyzed bouts was matched from both groups for a given experimental repeat to ensure an identical representation of control and condition bouts. Individual bouts were aligned at the time of peak speed. Bouts were excluded if their peak speed was <5mm/s or the fish rotated more than 30°(120°/sec) during the acceleration. The fractions excluded were as follows: for 7 dpf ablation: ctrl 0.2% lesion 0.15%; 7 dpf activation: ctrl 1% activation 1.7%; 14 dpf ablation dark: ctrl 0.05% ablation 0.05%; 14 dpf ablation light: ctrl 0.02% ablation 0.02%. For each experiment between 0.02% and 1.7% of bouts were excluded based on those criteria. Data was recorded either at 40Hz (activation experiments) or 160Hz (all other experiments). Effect size was calculated as the difference between the control value and the condition value relative to the control value. For fin body slope effect size the control value of the fast bin (i.e. largest slope) was used for effect size calculations to avoid overestimation of changes due to small control values.

Kinematic analyses proceeded as in<sup>20</sup>; key parameters were defined as follows:

- **Posture** is the pitch angle of the fish (long axis of the body relative to the horizon) at -250ms relative to peak speed, just before swim bout initiation. Positive values are nose-up.
- **Upward rotation** refers to the rotation from -250ms to the peak angular velocity; only bouts with positive upward rotation were included in the analysis of fin-body coordination.
- **Lift** is the residual change in depth (z) across a bout after subtracting the change expected from the posture of the fish as detailed in<sup>19</sup>. Briefly, the expected change is calculated using the distance the fish moves in x from -100 to 100ms and the pitch angle at -100ms. Only bouts with positive lift were included in the analysis of fin-body coordination.
- **Lift/rotation ratio** is defined as the slope of the best linear fit between upward rotation and lift across bouts. The goodness of fit,  $R^2$  was used as a measure of how well the fins and trunk are coordinated to generate lift, after<sup>19</sup>.

### Functional GCaMP imaging in Purkinje cells

All calcium imaging experiments were performed using Tilt In Place Microscopy (TIPM), described comprehensively in<sup>60</sup>. Briefly, 7 dpf fish were mounted in the center of the uncoated side of a mirror galvanometer (catalog #GVS0111, Thorlabs) in 2% low-melting- point agarose. E3 was placed over the agarose, and the galvanometer mirror was placed under the microscope. A microscope (Thorlabs Bergamo) was used to measure fluorescence elicited by multiphoton excitation (920nm) from a pulsed infrared laser (Mai Tai HP). Fast volumetric scanning was achieved using a piezo actuator (catalog #PFM450E, Thorlabs) to move the objective. Each frame of the volume (224 x 96 pixels) was collected

with a 0.6 ms pixel dwell time (19.1 frames/s) resulting in a sampling rate of 3.82 volumes/s. While this imaging rate might be too slow to distinguish single spikes, it is suitable to measure a difference in calcium transients upon pitch stimulation to nose-up or nose-down direction.

For eccentric imaging, for each cell 21 trials were recorded at  $\pm 30^\circ$  in blocks; the order of nose-up and nose-down blocks were alternated. After all 42 trials were recorded fish were anesthetized with 0.2 mg/ml MESAB; after 10 min the baseline fluorescence at  $\pm 30^\circ$  was recorded to establish a baseline that controlled for eccentricity. Analysis was done using Fiji and MATLAB. In total 43 Purkinje cells were imaged and 31 cells were kept from 8 fish. Only Purkinje cells that could be reliably identified at  $\pm 30^\circ$  were analyzed.

Regions of interest were drawn in Fiji and loaded into MATLAB to extract the intensity of fluorescence after motion correction was performed<sup>97</sup>. The integral of each stimulus was calculated and trials of the same direction were averaged as the tonic response to  $\pm 30^\circ$  pitch. To extract cells with directional information the directionality index (DI) was calculated by dividing the difference of the up and down responses by the sum of it. Cells with a DI greater than  $\pm 0.35$  were considered directionally tuned. Only Purkinje cells that were not directionally tuned were used for principal component analysis and subsequent support vector machine decoding analysis. The decoder was used with different population sizes using k-fold testing to avoid overfitting; permutations were performed on randomized data as a null hypothesis (5-fold cross-validation; 100 shuffles for randomization).

For calcium imaging in 7 and 14 dpf larvae, a horizontal imaging protocol was used. In total 11 fish were imaged at 7 dpf and 7 fish at 14 dpf. A total of 138/90 (7/14 dpf) cells were recorded. Cells were imaged while the fish was horizontal. Before each trial, a 15 sec period was recorded; the average activity during this time was used as the baseline. Fish were pitched nose-down ( $-19^\circ$ ) for 15s and rapidly returned to horizontal, whereupon calcium activity was measured. This stimulus was then repeated in the nose-up ( $+19^\circ$ ) direction. The maximum dFF of the first second upon return was analyzed. Cells were classified into directional or non-directional based on the directionality index as described above. PCA and decoder analyses were performed using activity from non-directional cells. Decoding accuracy was tested for each fish individually.

## Statistics

All statistical testing was done in Matlab R2020a. Unless otherwise mentioned two-sided Wilcoxon rank sum tests were performed for measured values. For fitted variables (slope and  $R^2$  of fin body correlation) we bootstrapped the data and calculated the bootstrapped p-value. Additionally, we only considered effect sizes of  $\geq 15\%$  to be biologically relevant.

## Data & Code

All data, raw and analyzed, as well as code necessary to generate the figures is available at the following DOI: 10.17605/OSF.IO/9X57Z

## ACKNOWLEDGMENTS

*Tg(aldoca:TRPV1-tagRFP)* fish were generated using a plasmid that was a gift from David Prober's laboratory. Research was supported by the National Institute on Deafness and Communication Disorders of the National Institutes of Health under award number R01DC017489. The authors would like to thank Martha Bagnall and Abigail Person along with the members of the Schoppik and Nagel lab for their valuable feedback and discussions.

## AUTHOR CONTRIBUTIONS

Conceptualization: FA and DS, Methodology: FA and DS, Investigation: FA and KN, Visualization: FA, Writing: FA, DS Editing: DS, Funding Acquisition: FA and DS, Supervision: DS, MH. *Tg(aldoca:TRPV1-tagRFP)* fish were generated by KM.

## AUTHOR COMPETING INTERESTS

The authors declare no competing interests.

## REFERENCES

1. James M. Sprague and William W. Chambers. Regulation of posture in intact and decerebrate cat: I. cerebellum, reticular formation, vestibular nuclei. *Journal of Neurophysiology*, 16(5):451–463, September 1953.
2. J. F. Kleine, Y. Guan, E. Kipiani, L. Glonti, M. Hoshi, and U. Büttner. Trunk position influences vestibular responses of fastigial nucleus neurons in the alert monkey. *Journal of Neurophysiology*, 91(5):2090–2100, May 2004.
3. M. E. Ioffe. Cerebellar control of posture. In *Handbook of the Cerebellum and Cerebellar Disorders*, pages 1221–1240. Springer Netherlands, 2013.
4. Shinichiro Tsutsumi, Oscar Chadney, Tin-Long Yiu, Edgar Bäumlner, Lavinia Faraggiana, Maxime Beau, and Michael Häusser. Purkinje cell activity determines the timing of sensory-evoked motor initiation. *Cell Reports*, 33(12):108537, December 2020.
5. Matthew I. Becker and Abigail L. Person. Cerebellar control of reach kinematics for endpoint precision. *Neuron*, 103(2):335–348.e5, July 2019.
6. Shane A. Heiney, Jinsook Kim, George J. Augustine, and Javier F. Medina. Precise control of movement kinematics by optogenetic inhibition of purkinje cell activity. *The Journal of Neuroscience*, 34(6):2321–2330, February 2014.
7. Jin Bo, Hannah J. Block, Jane E. Clark, and Amy J. Bastian. A cerebellar deficit in sensorimotor prediction explains movement timing variability. *Journal of Neurophysiology*, 100(5):2825–2832, November 2008.
8. Dana M. Darmohray, Jovin R. Jacobs, Hugo G. Marques, and Megan R. Carey. Spatial and temporal locomotor learning in mouse cerebellum. *Neuron*, 102(1):217–231.e4, April 2019.
9. F. B. Horak and H. C. Diener. Cerebellar control of postural scaling and central set in stance. *Journal of Neurophysiology*, 72(2):479–493, August 1994.
10. Susanne M. Morton, Ya-Weng Tseng, Kathleen M. Zackowski, Jaclyn R. Daline, and Amy J. Bastian. Longitudinal tracking of gait and balance impairments in cerebellar disease. *Movement Disorders*, 25(12):1944–1952, June 2010.

11. Ana S Machado, Dana M Darmohray, João Fayad, Hugo G Marques, and Megan R Carey. A quantitative framework for whole-body coordination reveals specific deficits in freely walking ataxic mice. *eLife*, 4, October 2015.
12. Keith Sheppard, Justin Gardin, Gautam S. Sabnis, Asaf Peer, Megan Darrell, Sean Deats, Brian Geuther, Cathleen M. Lutz, and Vivek Kumar. Stride-level analysis of mouse open field behavior using deep-learning-based pose estimation. *Cell Reports*, 38(2):110231, January 2022.
13. Ana S Machado, Hugo G Marques, Diogo F Duarte, Dana M Darmohray, and Megan R Carey. Shared and specific signatures of locomotor ataxia in mutant mice. *eLife*, 9, July 2020.
14. Dick Jaarsma, Maria B. Birksdóttir, Randy van Vossen, Demi W.G.D. Oomen, Oussama Akhiyat, Wilbert P. Vermeij, Sebastiaan K.E. Koekkoek, Chris I. De Zeeuw, and Laurens W.J. Bosman. Different purkinje cell pathologies cause specific patterns of progressive ataxia in mice. *bioRxiv*, August 2023.
15. Erich Von Holst. *The behavioural physiology of animals and man: the collected papers of Erich von Holst*, volume 1. University of Miami Press, 1973.
16. M. Sfakiotakis, D.M. Lane, and J.B.C. Davies. Review of fish swimming modes for aquatic locomotion. *IEEE Journal of Oceanic Engineering*, 24(2):237–252, April 1999.
17. David E. Ehrlich and David Schoppik. Control of movement initiation underlies the development of balance. *Current Biology*, 27(3):334–344, February 2017.
18. David E. Ehrlich and David Schoppik. A novel mechanism for volitional locomotion in larval zebrafish. *bioRxiv*, September 2017.
19. David E Ehrlich and David Schoppik. A primal role for the vestibular sense in the development of coordinated locomotion. *eLife*, 8, October 2019.
20. Yunlu Zhu, Franziska Auer, Hannah Gelnaw, Samantha N. Davis, Kyla R. Hamling, Christina E. May, Hassan Ahamed, Niels Ringstad, Katherine I. Nagel, and David Schoppik. SAMPL is a high-throughput solution to study unconstrained vertical behavior in small animals. *Cell Reports*, 42(6):112573, June 2023.
21. Sol Pose-Méndez, Paul Schramm, Komali Valishetti, and Reinhard W. Köster. Development, circuitry, and function of the zebrafish cerebellum. *Cellular and Molecular Life Sciences*, 80(8), July 2023.
22. Masahiko Hibi and Takashi Shimizu. Development of the cerebellum and cerebellar neural circuits. *Developmental Neurobiology*, 72(3):282–301, February 2012.
23. Lucy A. Heap, Chi Ching Goh, Karin S. Kassahn, and Ethan K. Scott. Cerebellar output in zebrafish: An analysis of spatial patterns and topography in eurydendroid cell projections. *Frontiers in Neural Circuits*, 7, 2013.
24. Hideaki Matsui, Kazuhiko Namikawa, Andreas Babaryka, and Reinhard W. Köster. Functional regionalization of the teleost cerebellum analyzed in vivo. *Proceedings of the National Academy of Sciences*, 111(32):11846–11851, July 2014.
25. Thomas C Harmon, Uri Magaram, David L McLean, and Indira M Raman. Distinct responses of purkinje neurons and roles of simple spikes during associative motor learning in larval zebrafish. *eLife*, 6, May 2017.
26. Alessandro Dorigo, Komali Valishetti, Florian Hetsch, Hideaki Matsui, Jochen C. Meier, Kazuhiko Namikawa, and Reinhard W. Köster. Functional regionalization of the differentiating cerebellar purkinje cell population occurs in an activity-dependent manner. *Frontiers in Molecular Neuroscience*, 16, April 2023.
27. Laura D. Knogler, Daniil A. Markov, Elena I. Dragomir, Vilim Štih, and Ruben Portugues. Sensorimotor representations in cerebellar granule cells in larval zebrafish are dense, spatially organized, and non-temporally patterned. *Current Biology*, 27(9):1288–1302, May 2017.
28. Sherika J. G. Sylvester, Melanie M. Lee, Alexandre D. Ramirez, Sukbin Lim, Mark S. Goldman, and Emre R. F. Aksay. Population-scale organization of cerebellar granule neuron signaling during a visuomotor behavior. *Scientific Reports*, 7(1), November 2017.
29. Weipang Chang, Andrea Pedroni, Reinhard W. Köster, Stefania Giacomello, and Konstantinos Ampatzis. Purkinje cells located in the adult zebrafish valvula cerebelli exhibit variable functional responses. *Scientific Reports*, 11(1), September 2021.
30. Misha B. Ahrens, Jennifer M. Li, Michael B. Orger, Drew N. Robson, Alexander F. Schier, Florian Engert, and Ruben Portugues. Brain-wide neuronal dynamics during motor adaptation in zebrafish. *Nature*, 485(7399):471–477, May 2012.
31. Mohini Sengupta and Vatsala Thirumalai. AMPA receptor mediated synaptic excitation drives state-dependent bursting in purkinje neurons of zebrafish larvae. *eLife*, 4, September 2015.
32. Karina Scalise, Takashi Shimizu, Masahiko Hibi, and Nathaniel B. Sawtell. Responses of cerebellar purkinje cells during fictive optomotor behavior in larval zebrafish. *Journal of Neurophysiology*, 116(5):2067–2080, November 2016.
33. Laura D Knogler, Andreas M Kist, and Ruben Portugues. Motor context dominates output from purkinje cell functional regions during reflexive visuomotor behaviours. *eLife*, 8, January 2019.
34. Thomas C. Harmon, David L. McLean, and Indira M. Raman. Integration of swimming-related synaptic excitation and inhibition by olig2+ eurydendroid neurons in larval zebrafish cerebellum. *The Journal of Neuroscience*, 40(15):3063–3074, March 2020.
35. Qian Lin, Jason Manley, Magdalena Helmreich, Friederike Schlumm, Jennifer M. Li, Drew N. Robson, Florian Engert, Alexander Schier, Tobias Nöbauer, and Alipasha Vaziri. Cerebellar neuromechanics predict decision timing and outcome on the single-trial level. *Cell*, 180(3):536–551.e17, February 2020.
36. Ot Prat, Luigi Petrucco, Vilim tih, and Ruben Portugues. Comparing the representation of a simple visual stimulus across the cerebellar network. *bioRxiv*, September 2022.
37. Marion Najac, David L. McLean, and Indira M. Raman. Synaptic variance and action potential firing of cerebellar output neurons during motor learning in larval zebrafish. *Current Biology*, 33(16):3299–3311.e3, August 2023.
38. Sriram Narayanan, Aalok Varma, and Vatsala Thirumalai. Predictive neural computations in the cerebellum contribute to motor planning and faster behavioral responses in larval zebrafish. *Science Advances*, 10(1), January 2024.
39. Geoffrey Migault, Thijs L. van der Plas, Hugo Trentesaux, Thomas Panier, Raphaël Candelier, Rémi Proville, Bernhard Englitz, Georges Debrégeas, and Volker Bormuth. Whole-brain calcium imaging during physiological vestibular stimulation in larval zebrafish. *Current Biology*, 28(23):3723–3735.e6, December 2018.
40. Itia A. Favre-Bulle, Gilles Vanwalleggem, Michael A. Taylor, Halina Rubinsztein-Dunlop, and Ethan K. Scott. Cellular-resolution imaging of vestibular processing across the larval zebrafish brain. *Current Biology*, 28(23):3711–3722.e3, December 2018.
41. Blaine N. Armbruster, Xiang Li, Mark H. Pausch, Stefan Herlitze, and Bryan L. Roth. Evolving the lock to fit the key to create a family of g protein-coupled receptors potentially activated by an inert ligand. *Proceedings of the National Academy of Sciences*, 104(12):5163–5168, March 2007.
42. Francesca Prestori, Ileana Montagna, Egidio D'Angelo, and Lisa Mapelli. The optogenetic revolution in cerebellar investigations. *International Journal of Molecular Sciences*, 21(7):2494, April 2020.
43. Shane A. Heiney, Gregory J. Wojaczynski, and Javier F. Medina. Action-based organization of a cerebellar module specialized for predictive control of multiple body parts. *Neuron*, 109(18):2981–2994.e5, September 2021.
44. Michael A Gaffield, Britton A Sauerbrei, and Jason M Christie. Cerebellum encodes and influences the initiation, performance, and termination of discontinuous movements in mice. *eLife*, 11, April 2022.
45. Jessica L. Verpeut, Silke Bergeler, Mikhail Kislin, F. William Townes, Ugne Klibaite, Zahra M. Dhanerawala, Austin Hoag, Sanjeev Janarthanan, Caroline Jung, Junuk Lee, Thomas J. Pisano, Kelly M. Seagraves, Joshua W. Shaevitz, and Samuel S.-H. Wang. Cerebellar contributions to a brainwide network for flexible behavior in mice. *Communications Biology*, 6(1), June 2023.
46. Robijanto Soetedjo and Gregory D. Horwitz. Closed-loop optogenetic perturbation of macaque oculomotor cerebellum: evidence for an internal saccade model. *bioRxiv*, June 2023.
47. Ilaria Carta, Christopher H. Chen, Amanda L. Schott, Schnaude Dorizan, and Kamran Khodakhah. Cerebellar modulation of the reward circuitry and social behavior. *Science*, 363(6424), January 2019.
48. Xiaoying Chen, Yanhua Du, Gerard Joey Broussard, Mikhail Kislin, Carla M. Yuede, Shuwei Zhang, Sabine Dietmann, Harrison Gabel, Guoyan Zhao, Samuel S.-H. Wang, Xiaqing Zhang, and Azad Bonni. Transcriptomic mapping uncovers purkinje neuron plasticity driving learning. *Nature*, 605(7911):722–727, May 2022.
49. Skyler L Jackman, Christopher H Chen, Heather L Offermann, Iain R Drew, Bailey M Harrison, Anna M Bowman, Katelyn M Flick, Isabella Flaquer, and Wade G Regehr. Cerebellar purkinje cell activity modulates aggressive behavior. *eLife*, 9, April 2020.
50. Paula A. Zamudio, Dominic Gioia, Christina Glaser, and John J. Woodward. Chemogenetic perturbation of the posterior but not anterior cerebellum reduces voluntary ethanol consumption. *eneuro*, pages ENEURO.0037–23.2023, September 2023.

51. Owen Y. Chao, Ezequiel Marron Fernandez de Velasco, Salil Saurav Pathak, Swati Maitra, Hao Zhang, Lisa Duvick, Kevin Wickman, Harry T. Orr, Hirokazu Hirai, and Yi-Mei Yang. Targeting inhibitory cerebellar circuitry to alleviate behavioral deficits in a mouse model for studying idiopathic autism. *Neuropsychopharmacology*, 45(7):1159–1170, March 2020.
52. Owen Y. Chao, Hao Zhang, Salil Saurav Pathak, Joseph P. Huston, and Yi-Mei Yang. Functional convergence of motor and social processes in lobule IV/v of the mouse cerebellum. *The Cerebellum*, 20(6):836–852, March 2021.
53. Meike E. van der Heijden, Amanda M. Brown, Dominic J. Kizek, and Roy V. Sillitoe. Neural spiking signatures predict behavioral phenotypes of cerebellar movement disorders. *bioRxiv*, May 2023.
54. Juan L. Gomez, Jordi Bonaventura, Wojciech Lesniak, William B. Mathews, Polina Sysa-Shah, Lionel A. Rodriguez, Randall J. Ellis, Christopher T. Richie, Brandon K. Harvey, Robert F. Dannals, Martin G. Pomper, Antonello Bonci, and Michael Michaelides. Chemogenetics revealed: DREADD occupancy and activation via converted clozapine. *Science*, 357(6350):503–507, August 2017.
55. Shijia Chen, Cindy N Chiu, Kimberly L McArthur, Joseph R Fetcho, and David A Prober. TRP channel mediated neuronal activation and ablation in freely behaving zebrafish. *Nature Methods*, 13(2):147–150, December 2015.
56. Philia Gau, Jason Poon, Carmen Ufret-Vincenty, Corey D. Snelson, Sharona E. Gordon, David W. Raible, and Ajay Dhaka. The zebrafish ortholog of TRPV1 is required for heat-induced locomotion. *The Journal of Neuroscience*, 33(12):5249–5260, March 2013.
57. Jacob G Bernstein, Paul A Garrity, and Edward S Boyden. Optogenetics and thermogenetics: technologies for controlling the activity of targeted cells within intact neural circuits. *Current Opinion in Neurobiology*, 22(1):61–71, February 2012.
58. Kyla R. Hamling, Zachary J.C. Tobias, and Tamily A. Weissman. Mapping the development of cerebellar purkinje cells in zebrafish. *Developmental Neurobiology*, 75(11):1174–1188, February 2015.
59. Young-Ki Bae, Shuichi Kani, Takashi Shimizu, Koji Tanabe, Hideaki Nojima, Yukiko Kimura, Shin ichi Higashijima, and Masahiko Hibi. Anatomy of zebrafish cerebellum and screen for mutations affecting its development. *Developmental Biology*, 330(2):406–426, June 2009.
60. Kyla R. Hamling, Yunlu Zhu, Franziska Auer, and David Schoppik. Tilt in place microscopy: a simple, low-cost solution to image neural responses to body rotations. *The Journal of Neuroscience*, 43(6):936–948, December 2022.
61. M. Ito, M. Yoshida, and K. Obata. Monosynaptic inhibition of the intracerebellar nuclei induced from the cerebellar cortex. *Experientia*, 20(10):575–576, October 1964.
62. M. Ito, M. Yoshida, K. Obata, N. Kawai, and M. Udo. Inhibitory control of intracerebellar nuclei by the purkinje cell axons. *Experimental Brain Research*, 10(1):64–80, 1970.
63. Nadia L. Cermnarina and John A. Rawson. Evidence that climbing fibers control an intrinsic spike generator in cerebellar purkinje cells. *The Journal of Neuroscience*, 24(19):4510–4517, May 2004.
64. Meha P. Jadhav and Vatsala Thirumalai. Ionic conductances driving tonic firing in purkinje neurons of larval zebrafish. *bioRxiv*, December 2023.
65. Kyla R. Hamling, Katherine Harmon, Marie Greaney, Zoë Dobler, Yukiko Kimura, Shin ichi Higashijima, and David Schoppik. Synaptic encoding of vestibular sensation regulates movement timing and coordination. *bioRxiv*, July 2021.
66. Joanna Mattis, Kay M Tye, Emily A Ferenczi, Charu Ramakrishnan, Daniel J O'Shea, Rohit Prakash, Lisa A Gunaydin, Minsuk Hyun, Lief E Fenno, Viviana Gradinaru, Ofer Yizhar, and Karl Deisseroth. Principles for applying optogenetic tools derived from direct comparative analysis of microbial opsins. *Nature Methods*, 9(2):159–172, December 2011.
67. D. H. Heck, W. T. Thach, and J. G. Keating. On-beam synchrony in the cerebellum as the mechanism for the timing and coordination of movement. *Proceedings of the National Academy of Sciences*, 104(18):7658–7663, May 2007.
68. Abigail L. Person and Indira M. Raman. Purkinje neuron synchrony elicits time-locked spiking in the cerebellar nuclei. *Nature*, 481(7382):502–505, December 2011.
69. Abigail L. Person and Indira M. Raman. Synchrony and neural coding in cerebellar circuits. *Frontiers in Neural Circuits*, 6, 2012.
70. Kyung-Seok Han, Chong Guo, Christopher H. Chen, Laurens Witter, Tomas Osorno, and Wade G. Regehr. Ephaptic coupling promotes synchronous firing of cerebellar purkinje cells. *Neuron*, 100(3):564–578.e3, November 2018.
71. Hannah L Payne, Ranran L French, Christine C Guo, TD Barbara Nguyen-Vu, Tiina Manninen, and Jennifer L Raymond. Cerebellar purkinje cells control eye movements with a rapid rate code that is invariant to spike irregularity. *eLife*, 8, May 2019.
72. Abdulaheem Nashef, Michael S. Spindle, Dylan J. Calame, and Abigail L. Person. A dual purkinje cell rate and synchrony code sculpts reach kinematics. *bioRxiv*, July 2023.
73. David J. Herzfeld, Mati Joshua, and Stephen G. Lisberger. Rate versus synchrony codes for cerebellar control of motor behavior. *Neuron*, 111(15):2448–2460.e6, August 2023.
74. Zhikai Liu, Yukiko Kimura, Shin ichi Higashijima, David G.C. Hildebrand, Joshua L. Morgan, and Martha W. Bagnall. Central vestibular tuning arises from patterned convergence of otolith afferents. *Neuron*, 108(4):748–762.e4, November 2020.
75. Kyla R. Hamling, Katherine Harmon, and David Schoppik. The nature and origin of synaptic inputs to vestibulospinal neurons in the larval zebrafish. *eneuro*, 10(6):ENEURO.0090–23.2023, June 2023.
76. Kristen E. Severi, Ruben Portugues, João C. Marques, Donald M. O'Malley, Michael B. Orger, and Florian Engert. Neural control and modulation of swimming speed in the larval zebrafish. *Neuron*, 83(3):692–707, August 2014.
77. Wei-Chun Wang and David L. McLean. Selective responses to tonic descending commands by temporal summation in a spinal motor pool. *Neuron*, 83(3):708–721, aug 2014.
78. Tod R. Thiele, Joseph C. Donovan, and Herwig Baier. Descending control of swim posture by a midbrain nucleus in zebrafish. *Neuron*, 83(3):679–691, aug 2014.
79. Sandeep Kishore, Eli B. Cadoff, Moneeza A. Agha, and David L. McLean. Orderly compartmental mapping of premotor inhibition in the developing zebrafish spinal cord. *Science*, 370(6515):431–436, October 2020.
80. Kristen P. D'Elia, Hanna Hameedy, Dena Goldblatt, Paul Frazel, Mercer Kriese, Yunlu Zhu, Kyla R. Hamling, Koichi Kawakami, Shane A. Liddelow, David Schoppik, and Jeremy S. Dasen. Determinants of motor neuron functional subtypes important for locomotor speed. *Cell Reports*, 42(9):113049, September 2023.
81. Martin Carbo-Tano, Mathilde Lapoix, Xinyu Jia, Olivier Thouvenin, Marco Pascucci, François Auclair, Feng B. Quan, Shahad Albadri, Vernie Aguda, Younes Farouj, Elizabeth M. C. Hillman, Ruben Portugues, Filippo Del Bene, Tod R. Thiele, Réjean Dubuc, and Claire Wyart. The mesencephalic locomotor region recruits v2a reticulospinal neurons to drive forward locomotion in larval zebrafish. *Nature Neuroscience*, September 2023.
82. Yuto Uemura, Kagayaki Kato, Koichi Kawakami, Yukiko Kimura, Yoichi Oda, and Shin ichi Higashijima. Neuronal circuits that control rhythmic pectoral fin movements in zebrafish. *The Journal of Neuroscience*, 40(35):6678–6690, July 2020.
83. Urs L. Böhm, Yukiko Kimura, Takashi Kawashima, Misha B. Ahrens, Shin ichi Higashijima, Florian Engert, and Adam E. Cohen. Voltage imaging identifies spinal circuits that modulate locomotor adaptation in zebrafish. *Neuron*, 110(7):1211–1222.e4, April 2022.
84. Jamie D Costabile, Kaarthik A Balakrishnan, Sina Schwinn, and Martin Haesemeyer. Model discovery to link neural activity to behavioral tasks. *eLife*, 12, June 2023.
85. Omid A Zobeiri and Kathleen E Cullen. Distinct representations of body and head motion are dynamically encoded by purkinje cell populations in the macaque cerebellum. *eLife*, 11, April 2022.
86. Ehsan Sedaghat-Nejad, Jay S. Pi, Paul Hage, Mohammad Amin Fakharian, and Reza Shadmehr. Synchronous spiking of cerebellar purkinje cells during control of movements. *Proceedings of the National Academy of Sciences*, 119(14), March 2022.
87. Detlef H. Heck, Chris I. De Zeeuw, Dieter Jaeger, Kamran Khodakhah, and Abigail L. Person. The neuronal code(s) of the cerebellum. *The Journal of Neuroscience*, 33(45):17603–17609, November 2013.
88. Isaac H. Bianco, Leung-Hang Ma, David Schoppik, Drew N. Robson, Michael B. Orger, James C. Beck, Jennifer M. Li, Alexander F. Schier, Florian Engert, and Robert Baker. The tangential nucleus controls a gravito-inertial vestibulo-ocular reflex. *Current Biology*, 22(14):1285–1295, July 2012.
89. Takumi Sugioka, Masashi Tanimoto, and Shin ichi Higashijima. Biomechanics and neural circuits for vestibular-induced fine postural control in larval zebrafish. *Nature Communications*, 14(1), March 2023.
90. David Schoppik, Isaac H. Bianco, David A. Prober, Adam D. Douglass, Drew N. Robson, Jennifer M.B. Li, Joel S.F. Greenwood, Edward Soucy, Florian Engert, and Alexander F. Schier. Gaze-stabilizing central vestibular neurons project asymmetrically to extraocular motoneuron pools. *The Journal of Neuroscience*, 37(47):11353–11365, September 2017.
91. Chris I. De Zeeuw, Stephen G. Lisberger, and Jennifer L. Raymond. Diversity and dynamism in the cerebellum. *Nature Neuroscience*, 24(2):160–167, December 2020.

92. Koji Tanabe, Shuichi Kani, Takashi Shimizu, Young-Ki Bae, Takaya Abe, and Masahiko Hibi. Atypical protein kinase c regulates primary dendrite specification of cerebellar purkinje cells by localizing golgi apparatus. *The Journal of Neuroscience*, 30(50):16983–16992, December 2010.
93. Hideaki Nojima, Sophie Rothhämel, Takashi Shimizu, Cheol-Hee Kim, Shigenobu Yonemura, Florence L. Marlow, and Masahiko Hibi. Syntabulin, a motor protein linker, controls dorsal determination. *Development*, 137(6):923–933, March 2010.
94. Miki Takeuchi, Koji Matsuda, Shingo Yamaguchi, Kazuhide Asakawa, Nobuhiko Miyasaka, Pradeep Lal, Yoshihiro Yoshihara, Akihiko Koga, Koichi Kawakami, Takashi Shimizu, and Masahiko Hibi. Establishment of gal4 transgenic zebrafish lines for analysis of development of cerebellar neural circuitry. *Developmental Biology*, 397(1):1–17, January 2015.
95. Timothy W Dunn, Yu Mu, Sujatha Narayan, Owen Randlett, Eva A Naumann, Chao-Tsung Yang, Alexander F Schier, Jeremy Freeman, Florian Engert, and Misha B Ahrens. Brain-wide mapping of neural activity controlling zebrafish exploratory locomotion. *eLife*, 5, March 2016.
96. Johannes Schindelin, Ignacio Arganda-Carreras, Erwin Frise, Verena Kaynig, Mark Longair, Tobias Pietzsch, Stephan Preibisch, Curtis Rueden, Stephan Saalfeld, Benjamin Schmid, Jean-Yves Tinevez, Daniel James White, Volker Hartenstein, Kevin Eliceiri, Pavel Tomancak, and Albert Cardona. Fiji: an open-source platform for biological-image analysis. *Nature Methods*, 9(7):676–682, June 2012.
97. Eftychios A. Pnevmatikakis and Andrea Giovannucci. NoRMCorre: An online algorithm for piecewise rigid motion correction of calcium imaging data. *Journal of Neuroscience Methods*, 291:83–94, November 2017.

**Table 1:** Table 1: Behavior measurements 7 dpf Purkinje cell activation

	control median [95% CI]	activation median [95% CI]	effect [%]	p-value	significance
<b>pre activation</b>					
climb posture [°]	15.4 [15.1, 15.8]	16.1 [15.6, 16.4]	4	0.006	no
dive posture [°]	-12.9 [-13.2, -12.6]	-13.5 [-13.8, -13.3]	5	<0.001	no
bout duration [s]	0.2 [0.2, 0.2]	0.2 [0.2, 0.2]	0	<0.001	no
IEI [s]	1.4 [1.4, 1.4]	1.4 [1.4, 1.4]	2	<0.001	no
speed [mm/s]	12.5 [12.4, 12.6]	12.6 [12.5, 12.6]	0	0.831	no
slope slow [mm/°]	0.015 [0.013, 0.019]	0.013 [0.011, 0.015]	-5	0.08	no
slope medium [mm/°]	0.018 [0.017, 0.019]	0.017 [0.016, 0.018]	-2	0.15	no
slope fast [mm/°]	0.042 [0.038, 0.047]	0.041 [0.039, 0.044]	-2	0.33	no
<b>post activation</b>					
climb posture [°]	14.7 [14.0, 15.4]	19.0 [18.5, 19.7]	29	<0.001	yes
dive posture [°]	-16.6 [-16.9, -16.1]	-20.5 [-20.9, -20.1]	24	<0.001	yes
bout duration [s]	0.2 [0.2, 0.2]	0.2 [0.2, 0.2]	0	<0.001	no
IEI [s]	1.6 [1.5, 1.6]	1.6 [1.5, 1.6]	2	0.043	no
speed [mm/s]	12.7 [12.5, 12.8]	13.0 [12.9, 13.1]	3	<0.001	no
slope slow [mm/°]	0.011 [0.009, 0.014]	0.010 [0.008, 0.013]	-3	0.22	no
slope medium [mm/°]	0.019 [0.017, 0.021]	0.017 [0.015, 0.018]	-5	0.04	no
slope fast [mm/°]	0.039 [0.035, 0.042]	0.040 [0.037, 0.045]	3	0.73	no

**Table 2:** Table 2: Behavior measurements 7 dpf Purkinje cell lesion

	control median [95% CI]	lesion median [95% CI]	effect [%]	p-value	significance
<b>pre lesion</b>					
climb posture [°]	18.0 [17.6, 18.4]	19.0 [18.6, 19.4]	6	0.001	no
dive posture [°]	-11.9 [-12.1, -11.6]	-11.5 [-11.7, -11.3]	-3	0.25	no
bout duration [s]	0.2 [0.2, 0.2]	0.2 [0.2, 0.2]	4	0.001	no
IEI [s]	1.8 [1.8, 1.9]	1.7 [1.7, 1.8]	-4	<0.001	no
speed [mm/s]	11.3 [11.2, 11.4]	12.0 [11.9, 12.1]	6	<0.001	no
slope slow [mm/°]	0.004 [0.002, 0.005]	0.005 [0.003, 0.007]	4	0.89	no
slope medium [mm/°]	0.009 [0.008, 0.011]	0.003 [0.001, 0.004]	-14	<0.001	no
slope fast [mm/°]	0.046 [0.043, 0.050]	0.046 [0.042, 0.050]	1	0.48	no
<b>post lesion</b>					
climb posture [°]	10.0 [9.5, 10.7]	13.6 [13.1, 14.3]	36	<0.001	yes
dive posture [°]	-11.7 [-11.9, -11.5]	-11.2 [-11.4, -11.0]	-4	0.002	no
bout duration [s]	0.2 [0.2, 0.2]	0.1 [0.1, 0.1]	-4	<0.001	no
IEI [s]	1.7 [1.7, 1.8]	1.7 [1.7, 1.7]	-2	0.20	no
speed [mm/s]	10.3 [10.2, 10.4]	10.6 [10.5, 10.7]	2	<0.001	no
slope slow [mm/°]	0.008 [0.007, 0.010]	0.005 [0.004, 0.006]	-8	<0.001	no
slope medium [mm/°]	0.012 [0.012, 0.013]	0.009 [0.008, 0.010]	-8	<0.001	no
slope fast [mm/°]	0.046 [0.041, 0.049]	0.026 [0.023, 0.031]	-43	<0.001	yes

**Table 3:** Table 3: Behavior measurements 14 dpf Purkinje cell lesion

	control median [95% CI]	lesion median [95% CI]	effect [%]	p-value	significance
<b>pre lesion</b>					
climb posture [°]	16.0 [15.6, 16.5]	15.2 [14.7, 15.9]	-5	<0.001	no
dive posture [°]	-9.0 [-9.4, -8.7]	-9.5 [-9.7, -9.1]	5	0.006	no
bout duration [s]	0.2 [0.2, 0.2]	0.2 [0.2, 0.2]	3	0.59	no
IEI [s]	2.3 [2.3, 2.3]	2.4 [2.4, 2.4]	4	0.29	no
speed [mm/s]	10.2 [10.0, 10.3]	10.5 [10.4, 10.7]	4	<0.001	no
<b>post lesion</b>					
climb posture [°]	14.3 [13.8, 14.8]	17.1 [16.2, 17.8]	20	<0.001	yes
dive posture [°]	-9.8 [-10.1, -9.5]	-12.3 [-12.6, -11.9]	26	<0.001	yes
bout duration [s]	0.2 [0.2, 0.2]	0.2 [0.2, 0.2]	-8	<0.001	no
IEI [s]	2.9 [2.8, 3.0]	2.8 [2.7, 2.8]	-4	0.01	no
speed [mm/s]	9.7 [9.6, 9.8]	9.3 [9.2, 9.4]	-3	<0.001	no

**Table 4:** Table 4: Behavior measurements 14 dpf Purkinje cell lesion

	control median [95% CI]	lesion median [95% CI]	effect [%]	p-value	significance
<b>lesion</b>					
slope slow [mm/°]	0.028 [0.022, 0.034]	0.028 [0.020, 0.037]	0	0.51	no
slope medium [mm/°]	0.053 [0.045, 0.061]	0.029 [0.022, 0.032]	-36	<0.001	yes
slope fast [mm/°]	0.066 [0.056, 0.080]	0.046 [0.038, 0.056]	-31	<0.001	yes
R <sup>2</sup> slow	0.125 [0.086, 0.173]	0.138 [0.076, 0.203]	5	0.58	no
R <sup>2</sup> medium	0.212 [0.159, 0.264]	0.080 [0.056, 0.104]	-53	<0.001	yes
R <sup>2</sup> fast	0.250 [0.198, 0.307]	0.150 [0.118, 0.197]	-40	0.01	yes

**Table 5:** Table 5: Behavior measurements 14 dpf pectoral fin amputation

	control median [95% CI]	fin amputation median [95% CI]	effect [%]	p-value	significance
<b>fin amputation</b>					
slope slow [mm/s]	0.032 [0.026, 0.039]	-0.005 [-0.008, -0.002]	-50	<0.001	yes
slope medium [mm/s]	0.058 [0.050, 0.065]	-0.004 [-0.006, -0.003]	-86	<0.001	yes
slope fast [mm/s]	0.073 [0.059, 0.085]	0.019 [0.015, 0.025]	-74	<0.001	yes
R <sup>2</sup> slow	0.137 [0.092, 0.189]	0.017 [0.003, 0.037]	-49	<0.001	yes
R <sup>2</sup> medium	0.211 [0.161, 0.248]	0.011 [0.003, 0.019]	-83	<0.001	yes
R <sup>2</sup> fast	0.242 [0.172, 0.287]	0.090 [0.053, 0.144]	-63	<0.001	yes



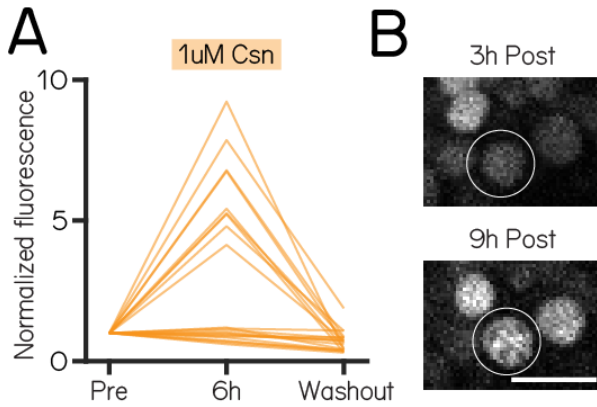


**Figure S1: Chemogenetic activation of Purkinje cells is reversible.**  
**(A)** Normalized change in fluorescence following treatment with 1  $\mu$ M capsaicin at 6h post treatment and after washout in individual Purkinje cells from *Tg(aldoca:TRPV1-tagRFP);Tg(elavl3:h2b-GCaMP6f)* larvae.  
**(B)** Example confocal image of Purkinje cell nuclei after 3 and 9h of 1  $\mu$ M capsaicin treatment. Speckled fluorescence could be observed after 9h of 1  $\mu$ M capsaicin treatment indicative of cell death (white circle). Scale bar 10  $\mu$ m.

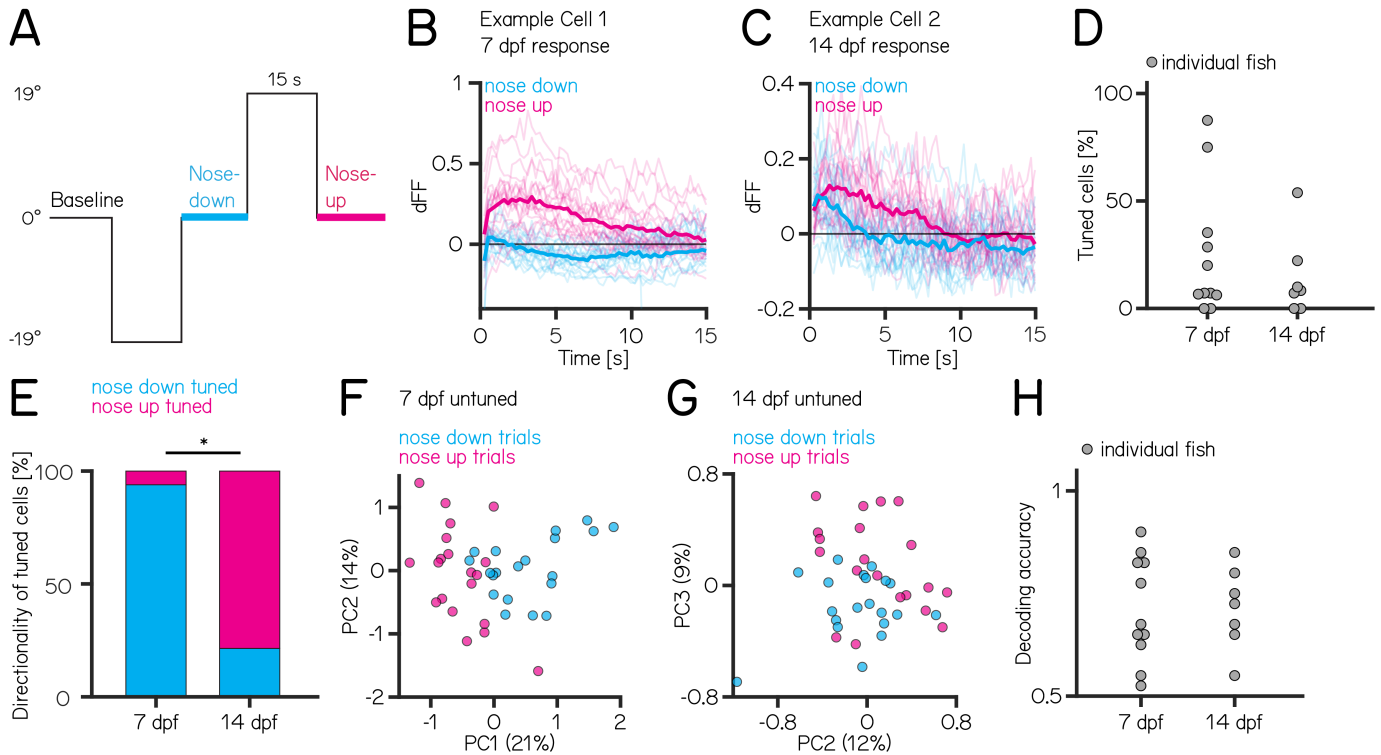


**Figure S2: Purkinje cell tuning direction shifts across development, population coding strength remains stable.**  
**(A)** One trial consisted of rapid galvanometer steps for 15 seconds in the nose down ( $-19^\circ$ , blue) and nose-up ( $+19^\circ$ , pink) direction.  
**(B)** Example responses ( $n=40$ ) from a single Purkinje cell at 7 dpf to nose-down (blue) and nose-up (pink) pitch tilts. The thicker lines indicate the median response to all nose-down or nose-up trials.  
**(C)** Example responses ( $n=40$ ) from a single Purkinje cell at 14 dpf to nose-down (blue) and nose-up (pink) pitch tilts. The thicker lines indicate the median response to all nose-down or nose-up trials.  
**(D)** Percentage of tuned cells from individual fish based on a directionality index larger than  $\pm 0.35$  (median (interquartile range): 7 dpf: 7 (6-34)%; 14 dpf: 8 (2-19)%;  $p$ -value = 0.7763, Wilcoxon rank sum test).  
**(E)** Direction of tuned cells at 7 and 14 dpf (7 dpf: 2/31 cells up/down-tuned; 14 dpf 11/3 cells up/down-tuned,  $p$ -value < 0.001, Fisher's exact test).  
**(F)** Principal component analysis of all untuned cells at 7 dpf for each of 20 up (pink) and 20 down (blue) trials. (Percentage of variance explained) **(G)** Principal component analysis of all untuned cells at 14 dpf for each of 20 up (pink) and 20 down (blue) trials. (Percentage of variance explained) **(H)** Performance of a support vector machine for binary classification of up/down tilt using the responses from untuned neurons. Dots are individual fish at 7 dpf and 14 dpf (median (interquartile range): 7 dpf: 0.68 (0.63-0.83); 14 dpf: 0.73 (0.65-0.79);  $p$ -value = 0.9468, Wilcoxon rank sum test).